

Spring 2005

Modeling and Slew-Maneuver Control of a Flexible Spacecraft

Jeremy E. Eckhart

Embry-Riddle Aeronautical University - Daytona Beach

Follow this and additional works at: <https://commons.erau.edu/db-theses>



Part of the [Space Vehicles Commons](#)

Scholarly Commons Citation

Eckhart, Jeremy E., "Modeling and Slew-Maneuver Control of a Flexible Spacecraft" (2005). *Theses - Daytona Beach*. 52.

<https://commons.erau.edu/db-theses/52>

This thesis is brought to you for free and open access by Embry-Riddle Aeronautical University – Daytona Beach at ERAU Scholarly Commons. It has been accepted for inclusion in the Theses - Daytona Beach collection by an authorized administrator of ERAU Scholarly Commons. For more information, please contact commons@erau.edu.

**MODELING AND SLEW-MANEUVER CONTROL OF A FLEXIBLE
SPACECRAFT**

By

Jeremy E. Eckhart

A thesis submitted to the Physical Sciences Department
In Partial Fulfillment of the Requirements of
Master of Science in Space Science

Embry-Riddle Aeronautical University
Daytona Beach, FL 32114
Spring 2005

UMI Number: EP32047

INFORMATION TO USERS

The quality of this reproduction is dependent upon the quality of the copy submitted. Broken or indistinct print, colored or poor quality illustrations and photographs, print bleed-through, substandard margins, and improper alignment can adversely affect reproduction.

In the unlikely event that the author did not send a complete manuscript and there are missing pages, these will be noted. Also, if unauthorized copyright material had to be removed, a note will indicate the deletion.

UMI[®]

UMI Microform EP32047
Copyright 2011 by ProQuest LLC
All rights reserved. This microform edition is protected against
unauthorized copying under Title 17, United States Code.

ProQuest LLC
789 East Eisenhower Parkway
P.O. Box 1346
Ann Arbor, MI 48106-1346

Copyright by Jeremy Eckhart 2005
All Rights Reserved

**MODELING AND SLEW-MANEUVER CONTROL OF A FLEXIBLE
SPACECRAFT**

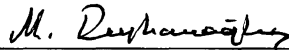
By Jeremy Eckhart

This thesis was prepared under the direction of the candidate's thesis committee chair,
Dr. Mahmut Reyhanoglu, Department of Physical Sciences, and has been approved by the
members of his thesis committee. It was submitted to the Department of Physical
Sciences and was accepted in partial fulfillment of the requirements for the

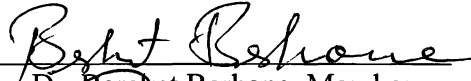
Degree of

Master of Science in Space Sciences

THESIS COMMITTEE:






Dr. Mahmut Reyhanoglu, Chair



Dr. Bereket Berhane, Member



Dr. Robert Fleck, Member


MSSPS Graduate Program Coordinator
Department Chair, Physical Sciences
Associate Chancellor, Daytona Beach Campus

2 May '05
Date

Acknowledgments

I first wish to thank Dr. Reyhanoglu for his guidance through this endeavor. Without his wisdom and support, this thesis never would have been completed.

I would also like to thank my parents, Ed and Diane, who have always believed in me. Even when I thought that I would never finish this thesis, their never-ending encouragement kept me going.

Abstract

Slew-maneuver control problem is studied for a flexible spacecraft consisting of a rigid main body to which a long flexible appendage is attached. Nonlinear dynamical system models are developed using both distributed parameter modeling and discrete parameter modeling; these models are shown to be equivalent for appropriately chosen system parameters. Lyapunov-based nonlinear feedback controllers are designed for the control of rigid-body motion while suppressing the lowest frequency vibrational mode. In case of large-angle maneuvers, these nonlinear controllers are shown to outperform the linearization-based controllers including the filtered proportional-derivative (PD) controllers as well as the linear quadratic regulator (LQR) controllers. Finally, the theoretical development is applied to a benchmark flexible system and a number of computer simulations are included to illustrate the results.

Table of Contents

Acknowledgements	iv
Abstract	v
Table of Contents	vi
List of Figures	viii
List of Tables	ix
Chapter I Introduction	1
1.1 Introduction	1
1.2 Literature Review	2
1.3. Contribution of Thesis	5
1.4. Organization of Thesis	5
Chapter II Mathematical Model	6
2.1 Introduction	6
2.2 Distributed Parameter Modeling	7
2.3 Discrete Parameter Modeling	12
Chapter III Review of Controller Design Methods	16
3.1 Introduction	16
3.2 System Stability	16
3.3 Lyapunov's Direct Method	18
3.4 Filters	19
3.4.1 Notch Filter	20
3.4.2 IIR Filter	21

3.5 Linear Quadratic Regulator	22
Chapter IV Controller Design	24
4.1 Introduction	24
4.2 A PD Controller with Notch Filter	24
4.3 A PD Controller with IIR Filter	26
4.4 LQR	27
4.5 Lyapunov-Based Design	29
Chapter V Experimental Setup	31
5.1 Introduction	31
5.2 Mathematical Model of Actuator Dynamics	32
5.3 Physical Values for the Experimental Setup	34
5.4 Application of Control Methods	36
Chapter VI Discussion of Results	62
6.1 Introduction	62
6.2 Case 1: Filtered Control	62
6.3 Case 1: LQR Control	63
6.4 Case 1: Lyapunov-Based Control	63
6.5 Case 2: Filtered Control	64
6.6 Case 2: LQR Control	65
6.7 Case 2: Lyapunov-Based Control	65
Chapter VII Conclusion	67
Bibliography	68

List of Figures

Figure 1.1. Example of a flexible structure, the LANDSAT 7 satellite with deployed solar array.	1
Figure 2.1. Diagram of continuous mass model of a spacecraft.	7
Figure 2.2. Basic model of the satellite undergoing a rotation and flexing.	12
Figure 3.1. Stable and unstable systems.	17
Figure 3.2. Example of a Lyapunov function.	19
Figure 3.3. Block diagram of a PD controlled system.	20
Figure 3.4. Block diagram of notch filter applied to a PD controlled system.	21
Figure 3.5. IIR filter applied to a PD controlled system.	22
Figure 5.1. The flexible link module setup.	31
Figure 5.2. Case 1 PD Control with Notch filter θ and $\dot{\theta}$ responses.	38
Figure 5.3. Case 1 PD Control with Notch filter q and \dot{q} responses.	39
Figure 5.4. Case 1 PD Control with Notch filter τ and V_i responses.	40
Figure 5.5. Case 1 PD Control with IIR filter θ and $\dot{\theta}$ responses.	41
Figure 5.6. Case 1 PD Control with IIR filter q and \dot{q} responses.	42
Figure 5.7. Case 1 PD Control with IIR filter τ and V_i responses.	43
Figure 5.8. Case 1 LQR method θ and $\dot{\theta}$ responses.	44
Figure 5.9. Case 1 LQR method q and \dot{q} responses.	45
Figure 5.10. Case 1 LQR method τ and V_i responses.	46
Figure 5.11. Case 1 Lyapunov method θ and $\dot{\theta}$ responses.	47
Figure 5.12. Case 1 Lyapunov method q and \dot{q} responses.	48

Figure 5.13. Case 1 Lyapunov method τ and V_i responses.	49
Figure 5.14. Case 2 PD Control with Notch filter θ and $\dot{\theta}$ responses.	50
Figure 5.15. Case 2 PD Control with Notch filter q and \dot{q} responses.	51
Figure 5.16. Case 2 PD Control with Notch filter τ and V_i responses.	52
Figure 5.17. Case 2 PD Control with IIR filter θ and $\dot{\theta}$ responses.	53
Figure 5.18. Case 2 PD Control with IIR filter q and \dot{q} responses.	54
Figure 5.19. Case 2 PD Control with IIR filter τ and V_i responses.	55
Figure 5.20. Case 2 LQR method θ and $\dot{\theta}$ responses.	56
Figure 5.21. Case 2 LQR method q and \dot{q} responses.	57
Figure 5.22. Case 2 LQR method τ and V_i responses.	58
Figure 5.23. Case 2 Lyapunov method θ and $\dot{\theta}$ responses.	59
Figure 5.24. Case 2 Lyapunov method q and \dot{q} responses.	60
Figure 5.25. Case 2 Lyapunov method τ and V_i responses.	61

List of tables

Table 5.1. Flexible arm parameters.	34
Table 5.2. Servo motor parameters.	35
Table 5.3. Initial conditions for test cases.	36
Table 5.4. Controller parameters.	37

Chapter I

Introduction

1.1 Introduction

Since the beginning of satellite design, manufactures have pushed the technological limits of material science to develop stronger and lighter materials for spacecraft construction. The demands placed on satellites utilizing this progress with the technology allows for the satellites to be larger than ever before. Controlling the appendages on large satellites is becoming much more difficult with this increased size. The materials used in the construction of spacecraft appendages, such as solar panels, are becoming more advanced so control systems have to be designed so the appendages do not become flexed or stressed to the point of failure. In addition to structural failures, the vibrations of the appendages can interfere with the normal operations of the satellite causing undesired motions of the spacecraft.

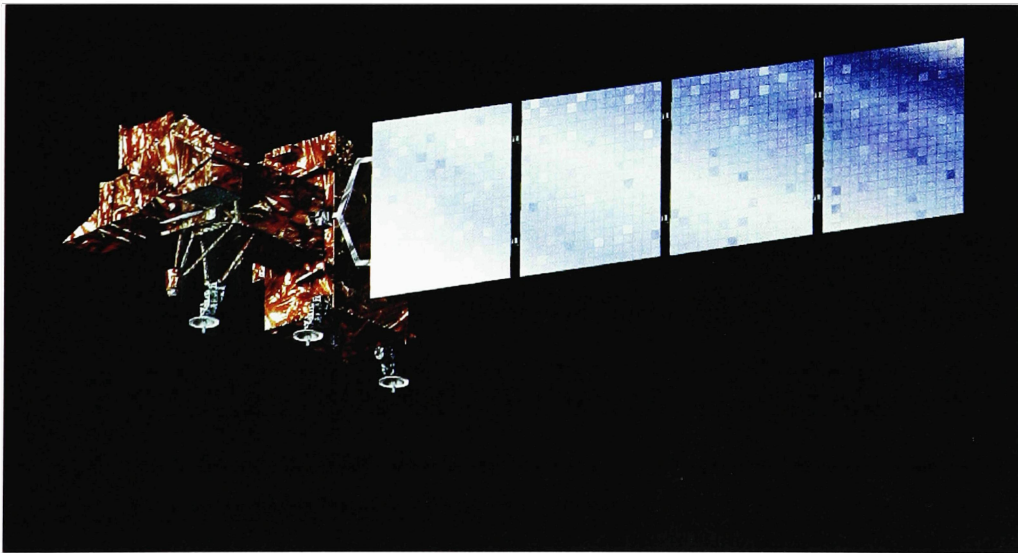


Figure 1: Example of a flexible structure, the LANDSAT 7 satellite with deployed solar array. ([gsfc.nasa.gov](https://www.gsfc.nasa.gov))

Development of control systems for rigid body spacecraft with flexible appendages provides a complex nonlinear control problem. For many years, many approaches have been taken to solve this problem. Many of the approaches only take into account the rigid body and flexible mode dynamics of the spacecraft. By ignoring the dynamics of an actual actuator system to control the system, the final controller design is incomplete for practical applications for active spacecraft.

Several controller designs have been considered over the years to tackle this complex problem. This thesis is aimed at providing a simple solution for the above-mentioned complex nonlinear control problem using Lyapunov's direct method in comparison to other control methods. Two separate Proportional Derivative controllers will be used combined with a Notch filter and an Infinite Impulse Response filter respectively. These filters are applied to insure that the inputs at certain frequencies are not passed through the filter to the system. The Linear Quadratic Regulator is another control method that will be applied to the system for comparison to the Lyapunov-Based design. Finally, the Lyapunov-based design is applied to the system. All of the designs will be tested over two test cases with differing initial conditions to test the capability of each model to perform the required maneuver.

1.2 Literature Review

An important area where flexible structure control finds a widespread use is in control of aerospace systems. An extensive amount of research has been done in the area of active vibration control in aerospace structures such as flexible satellites, space antennae, and

more recently the International Space Station (ISS). Some studies have focused on rotational maneuver of flexible spacecraft that is modeled as a rigid body to which flexible appendages such as solar panels or antennae are attached.

The book by Junkins and Kim [17] addresses in detail the problems associated with modeling and control of flexible structures. Infinite-dimensional models of flexible structures are treated using both Lagrangian approach and extended Hamilton's principle. The two most common approximate methods for finite dimensional models, the assumed modes methods and the finite element method, are thoroughly discussed. The book [17] also provides a detailed treatment of linear state feedback and output feedback problems associated with flexible structures. The book by Bryson [2] treats extensively several linear control design methods, including LQR (Linear Quadratic Regulator) and LQG (Linear Quadratic Gaussian) methods, for flexible spacecraft. Fundamentals of control theory can be found in [31]. The papers [18]-[20] provide mathematical models and control methodologies for multibody flexible space structures.

An experimental apparatus for investigating control laws for large flexible spacecraft is introduced by Cannon and Rosenthal [3]. The experimental work in this paper demonstrates the difficulties associated with active control of large space structures, particularly when the sensors and actuators are noncolocated. Such systems have many low-frequency vibration modes and very low inherent damping so that quite sophisticated techniques are needed for fast, stable, and robust control. Casella et al [4] discuss the problem of modeling and simulation of a laboratory structure (a lab model of a large

space structure, a large modular truss suspended by soft springs) equipped with both air jet thrusters and piezoactuators. Neat et al in [29] implements a vibration control strategy for spaceborne optical interferometers on a Micro-Precision Interferometer testbed. The strategy incorporates the high-frequency attenuation of six-axis vibration isolation with low-frequency attenuation of active optical control. Lim et al in [23] compare various controller designs for an experimental flexible structure.

In the literature, there have been many control schemes proposed for rotational maneuvers of flexible spacecraft with simultaneous vibration suppression. Control methods based on input command pre-shaping and/or time-delay filtering can be found in [1], [9], [13], [33]-[35], and references therein. Boundary feedback control laws are proposed in [5], [10]-[12], [21], [25]-[27]. These control laws employ Lyapunov theory for distributed parameter systems, i.e. systems described by partial differential equations; and the stability achieved by these laws holds for the original infinite dimensional systems. Boundary feedback control approaches provide a practical alternative to the control approach based on finite-dimensional models, which has the well-known drawbacks of mode truncation and possible spillover effects. Several types of controllers have been developed for flexible spacecraft, including variable structure controllers ([11], [14], [32]), controllers based on genetic algorithms [10], fuzzy logic controllers [28], and structurally stable controllers based on internal model principle [24]. Other control methods include bang-off-bang control [22], output feedback control [6]-[8], and dynamic dissipative control [15]-[16].

1.3. Contribution of Thesis

This thesis presents useful comparison of state-of-the-art linear and nonlinear control designs for a flexible spacecraft. The contribution of this thesis can be summarized as follows:

- Development of nonlinear dynamical system models using both distributed parameter modeling and discrete parameter modeling and showing their equivalence for appropriately chosen system parameters.
- Design of Lyapunov-based new nonlinear feedback controllers.
- Comparison of linearization-based controllers (filtered PD controllers and LQR controllers) and Lyapunov-based nonlinear feedback controllers.
- Application of the theoretical development to a benchmark flexible system testbed.

1.4. Organization of Thesis

The organization of the thesis is as follows. Chapter 2 gives the mathematical development of a model for a generic flexible system. Different controller designs are presented in Chapter 3. Chapter 4 introduces a benchmark flexible system model. Simulation results for the model are presented in Chapter 5. Controller comparisons are discussed in Chapter 6. Conclusions and future work are addressed in Chapter 7.

Chapter II

Mathematical Model

2.1 Introduction

A typical spacecraft structure consists of two principal parts: a main body and flexible appendages. The main body of the spacecraft contains all the payload instrumentation and control hardware. Its structure must be rigid in order to withstand mechanical loads during the launch stage. The second part of the spacecraft structure consists of large flexible appendages, such as solar arrays and antennae, built from light materials in order to minimize their weight. These flexible appendages induce structural vibrations that interfere strongly with the rigid-body attitude dynamics. In order to achieve high precision attitude demands, the dynamic effects of flexible appendages have to be taken into account.

This chapter is primarily concerned with the mathematical modeling of a spacecraft consisting of a rigid central body to which a flexible beam-like appendage is attached. The appendage is clamped to the rigid body at one end and free at the other. We assume that the flexible beam performs only planar motion. The appendage is considered to be a uniform flexible beam, and we make the Euler-Bernoulli assumptions of negligible shear deformation and negligible distributed rotary inertia. Any effects from atmospheric drag are also ignored.

The most widely used modeling techniques include distributed parameter modeling, discrete parameter modeling, and finite element modeling. This chapter briefly describes the first two techniques. For full details on modeling of flexible structures, see [17].

2.2 Distributed Parameter Modeling

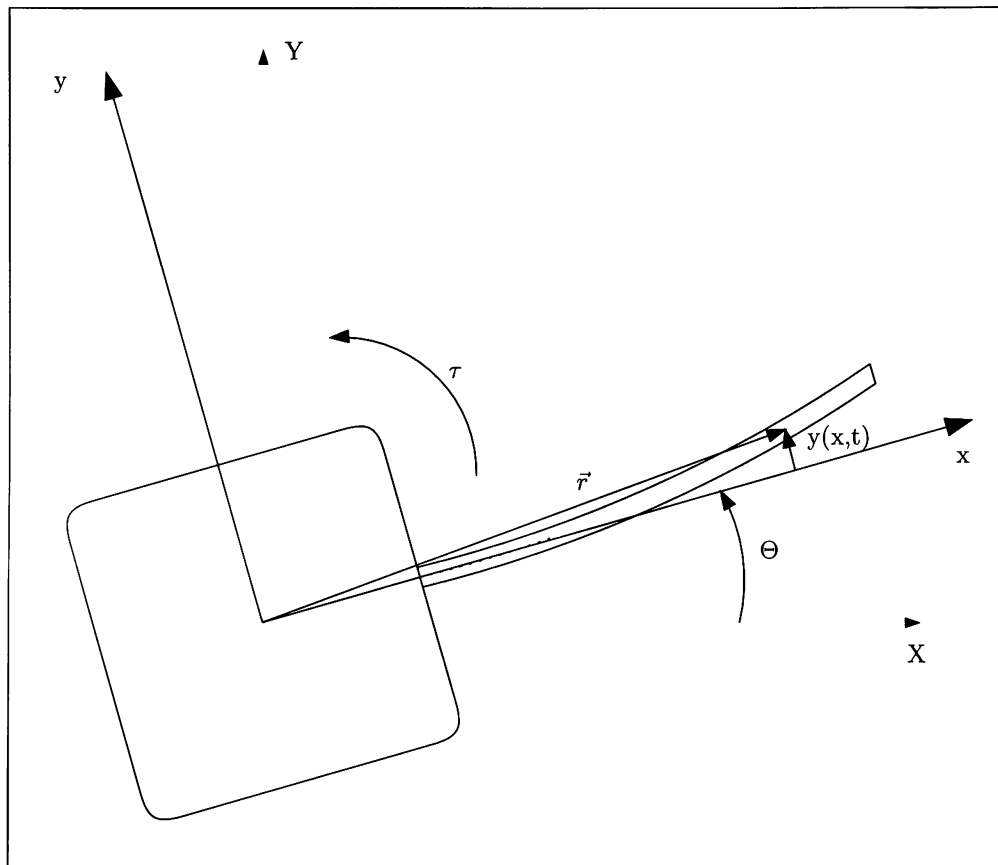


Figure 2.1. Diagram of continuous mass model of a spacecraft.

The use of distributed parameter modeling to model the panel of the spacecraft is commonly used in the development of controls for such systems. Consider a spacecraft model consisting of a rigid body and a single flexible panel modeled as an Euler-

Bernoulli beam as show in Figure 2.1. Let XYZ denote the inertial axes and xyz be the body-fixed axes. The axes xyz are assumed to be the principal axes of inertia. The angle θ represents the attitude of the spacecraft and τ is the control torque about the z axis.

Let ρ_l denote the mass per unit length of beam, I_z denote the rotational inertia of the rigid body about the z axis, and EI be the uniform flexural rigidity of the beam. Then the kinetic energy T and potential energy U can be expressed as:

$$T = \frac{1}{2} I_z \dot{\theta}^2 + \frac{1}{2} \int_0^l \rho_l \dot{\vec{r}}^2 dx \quad (2.1)$$

$$U = \frac{1}{2} EI \int_0^l (y'')^2 dx \quad (2.2)$$

where y or $y(x,t)$ denotes the deformation from the rigid body axis at a point x units along the beam and at time t , l is the length of the beam, θ denotes the attitude angle, and $\dot{\vec{r}}$ is the velocity of the beam at point x , which is derived below.

From the geometry, the position vector \vec{r} can be written as

$$\vec{r} = (x + l_0) \vec{i} + y \vec{j} \quad (2.3)$$

where l_0 is the distance from the spacecraft center of mass to the point of attachment of the beam.

Noting that the angular velocity of the rigid body is given by

$$\vec{\omega} = \dot{\theta} \vec{k} \quad (2.4)$$

the velocity vector $\dot{\vec{r}}$ can be computed as

$$\dot{\vec{r}} = \dot{y}\vec{j} + \dot{\theta}\vec{k} \times ((x+l_0)\vec{i} + y\vec{j}) \quad (2.5)$$

Here, assuming there is no deformation along the x axis, the \dot{x} term has been dropped.

Solving for $\dot{\vec{r}}^2$ yields:

$$\dot{\vec{r}}^2 = [(x+l_0)\dot{\theta} + \dot{y}]^2 + [y\dot{\theta}]^2 \quad (2.6)$$

Consequently, the Lagrangian $L = T - U$ can be expressed as

$$L = \frac{1}{2}I\dot{\theta}^2 + \frac{1}{2}\int_0^l \rho_l \left\{ (y\dot{\theta})^2 + [(x+l_0)\dot{\theta} + \dot{y}]^2 \right\} dx - \frac{1}{2}EI \int_0^l (y'')^2 dx \quad (2.7)$$

We use the assumed mode method to separate the variables for $y(x, t)$

$$y(x, t) = \sum_{k=1}^N \phi_k(x) q_k(t) \quad (2.8)$$

where $\phi_k(x)$ is the k^{th} shape function and $q_k(t)$ is the generalized coordinate corresponding to the k^{th} vibrational mode. As in [17], we use the following shape functions

$$\phi_k(x) = 1 - \cos\left(\frac{k\pi x}{l}\right) + \frac{1}{2}(-1)^{k+1} \left(\frac{k\pi x}{l}\right)^2 \quad (2.9)$$

It can be shown that these functions satisfy both the geometric ($y(0, t) = 0, y'(0, t) = 0$) and physical boundary conditions ($y''(l, t) = 0, y'''(l, t) = 0$), and thus they are comparison functions.

To obtain the simplest model, only the first mode will be considered, so $N = 1$. The substitution for $y(x, t)$ is as follows

$$y = \phi(x)q(t)$$

$$\dot{y} = \phi(x)\dot{q}(t)$$

$$y'' = \phi''(x)q(t)$$

The Lagrangian function then becomes

$$L = \frac{1}{2}I_z\dot{\theta}^2 + \frac{1}{2}\rho_l \int_0^l \left[\phi^2 q^2 \dot{\theta}^2 + (x+l_0)^2 \dot{\theta}^2 + \phi^2 \dot{q}^2 + 2(x+l_0)\dot{\theta}\phi\dot{q} \right] dx - \frac{1}{2}EI \int_0^l (\phi'')^2 q^2 dx \quad (2.10)$$

This can be simplified to the following expression

$$L = \frac{1}{2}I_t\dot{\theta}^2 + \frac{1}{2}m_q q^2 \dot{\theta}^2 + \frac{1}{2}m_q \dot{q}^2 + m_{\theta q} \dot{\theta}\dot{q} - \frac{1}{2}kq^2 \quad (2.11)$$

where

$$m_q = \rho_l \int_0^l \phi^2 dx$$

$$m_{\theta q} = \rho_l \int_0^l (x+l_0)\phi dx$$

$$k = EI \int_0^l (\phi'')^2 dx$$

$$I_t = I_z + \rho_l \left[(l+l_0)^3 - l_0^3 \right] / 3$$

The structural damping is included via the Rayleigh dissipation function given as

$$R = \frac{1}{2}c\dot{q}^2 \quad (2.12)$$

where c is the damping constant for the beam.

Consequently, applying Lagrange's equations

$$\begin{aligned}\frac{d}{dt} \frac{\partial L}{\partial \dot{\theta}} - \frac{\partial L}{\partial \theta} + \frac{\partial R}{\partial \dot{\theta}} &= \tau \\ \frac{d}{dt} \frac{\partial L}{\partial \dot{q}} - \frac{\partial L}{\partial q} + \frac{\partial R}{\partial \dot{q}} &= 0\end{aligned}$$

the equations of motion can be written as

$$\frac{d}{dt} [I_t \dot{\theta} + m_{\theta q} \dot{q} + m_q q^2 \dot{\theta}] = \tau \quad (2.13)$$

$$\frac{d}{dt} [m_q \dot{q} + m_{\theta q} \dot{\theta}] - m_q q \dot{\theta}^2 + kq + c\dot{q} = 0 \quad (2.14)$$

which can be expressed as

$$(I_t + m_q q^2) \ddot{\theta} + m_{\theta q} \ddot{q} + 2m_q q \dot{q} \dot{\theta} = \tau \quad (2.15)$$

$$m_q \ddot{q} + m_{\theta q} \ddot{\theta} - m_q q \dot{\theta}^2 + kq + c\dot{q} = 0 \quad (2.16)$$

Using a partial feedback linearization, we obtain

$$\ddot{\theta} = u \quad (2.17)$$

$$\ddot{q} + 2\xi\omega_n \dot{q} + \omega_n^2 q = -\alpha u + q \dot{\theta}^2 \quad (2.18)$$

where

$$u = \frac{\tau - m_{\theta q} q \dot{\theta}^2 + \alpha kq + \alpha c\dot{q} - 2m_q q \dot{q} \dot{\theta}}{I_t + m_q q^2 - \alpha m_{\theta q}} \quad (2.19)$$

$$\alpha = \frac{m_{\theta q}}{m_q} \quad (2.20)$$

$$\omega_n = \sqrt{\frac{k}{m_q}} \quad (2.21)$$

$$\xi = \frac{c}{2\sqrt{m_q k}} \quad (2.22)$$

Here u is the new control input, α is the coupling constant, ω_n is the natural frequency, and ξ is the damping ratio for the flexible appendage.

2.3 Discrete Parameter Modeling

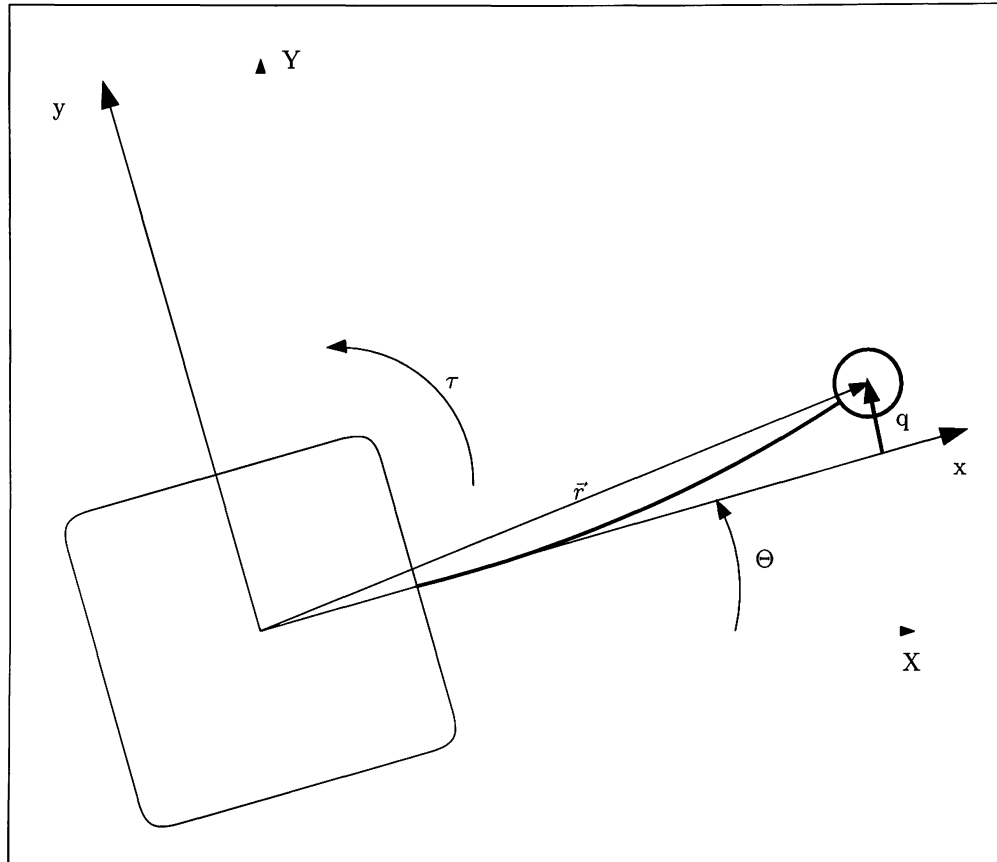


Figure 2.2. Basic model of the satellite undergoing a rotation and flexing.

Discrete parameter modeling is another useful method that can be applied to a combination spacecraft and flexible panel system. For the model, consider a spacecraft consisting of a rigid body and a flexible appendage. Here, a single mass model will be considered for the panel, i.e. the panel is modeled as a discrete mass at the end of a massless arm as shown in Figure 2.2. Let XYZ denote the inertial axes and xyz be the body-fixed axes. The axes xyz are assumed to be the principal axes of inertia.

Let \bar{m} denote the effective mass at the end of the beam, I_z denote the rotational inertia of the rigid body about the z axis, and k denote the stiffness coefficient of the panel. The angle θ represents the attitude of the spacecraft and τ is the control torque about the z axis.

Then the kinetic energy T and potential energy U can be expressed as:

$$T = \frac{1}{2} \bar{m} \dot{\bar{r}}^2 + \frac{1}{2} I_z \dot{\theta}^2 \quad (2.23)$$

$$U = \frac{1}{2} k q^2 \quad (2.24)$$

where q denotes the deformation from the rigid body axis x , θ denotes the attitude angle, and $\dot{\bar{r}}$ is the velocity of the point mass \bar{m} , which is derived below.

From the geometry, the position can be written as

$$\bar{r} = (l + l_0) \bar{i} + q \bar{j} \quad (2.25)$$

where l is the length of the panel and l_0 is the distance from the system center of mass to the point of attachment of the solar panel to the rigid body.

Recognizing that the angular velocity is given by

$$\bar{\omega} = \dot{\theta} \bar{k} \quad (2.26)$$

the velocity vector $\dot{\bar{r}}$ can be computed as

$$\dot{\bar{r}} = \dot{q} \bar{j} + \bar{\omega} \times \bar{r} = -q \dot{\theta} \bar{i} + (\dot{\theta} (l + l_0) + \dot{q}) \bar{j} \quad (2.27)$$

Finally squaring the $\dot{\vec{r}}$ vector yields

$$\dot{\vec{r}}^2 = q^2 \dot{\theta}^2 + \dot{q}^2 + 2(l+l_0)\dot{q}\dot{\theta} + (l+l_0)^2 \dot{\theta}^2 \quad (2.28)$$

Consequently, the Lagrangian $L = T - U$ can be expressed in terms of the generalized coordinates (θ, q) and generalized velocities $(\dot{\theta}, \dot{q})$ as

$$L = \frac{1}{2} \bar{m} \left[q^2 \dot{\theta}^2 + \dot{q}^2 + 2(l+l_0)\dot{q}\dot{\theta} + (l+l_0)^2 \dot{\theta}^2 \right] + \frac{1}{2} I_z \dot{\theta}^2 - \frac{1}{2} kq^2 \quad (2.29)$$

As in the previous section, let us define the Rayleigh dissipation function R as

$$R = \frac{1}{2} c \dot{q}^2 \quad (2.30)$$

where c is the mechanical dissipative constant.

Assuming a torque τ acts on the rigid hub, we can write the virtual work of the system as

$$\delta W = \tau \delta \theta \quad (2.31)$$

Consequently, applying Lagrange's equations

$$\frac{d}{dt} \frac{\partial L}{\partial \dot{\theta}} - \frac{\partial L}{\partial \theta} + \frac{\partial R}{\partial \dot{\theta}} = \tau \quad (2.32)$$

$$\frac{d}{dt} \frac{\partial L}{\partial \dot{q}} - \frac{\partial L}{\partial q} + \frac{\partial R}{\partial \dot{q}} = 0 \quad (2.33)$$

we obtain the equations of motion as

$$(I_z + \bar{m}q^2) \ddot{\theta} + \bar{m}(l+l_0) \ddot{q} + 2\bar{m}q\dot{q}\dot{\theta} = \tau \quad (2.34)$$

$$\bar{m}(l+l_0) \ddot{\theta} + \bar{m}\ddot{q} - \bar{m}q\dot{\theta}^2 + kq + c\dot{q} = 0 \quad (2.35)$$

where $I_z = I_z + \bar{m}(l+l_0)^2$. It is clear that, with $m_q = \bar{m}$, $m_{\theta q} = \bar{m}(l+l_0)$, these equations become identical to the equations of motion (2.15)-(2.16) derived in the previous section using distributed parameter modeling.

Using a partial feedback linearization, we obtain

$$\ddot{\theta} = u \quad (2.36)$$

$$\ddot{q} + 2\xi\omega_n\dot{q} + \omega_n^2q = -\alpha u + q\dot{\theta}^2 \quad (2.37)$$

where

$$u = \frac{\tau - \bar{m}(l+l_0)q\dot{\theta}^2 + (l+l_0)c\dot{q} + (l+l_0)kq - 2\bar{m}q\dot{q}\dot{\theta}}{I_z + \bar{m}q^2} \quad (2.38)$$

$$\alpha = l+l_0 \quad (2.39)$$

$$\omega_n = \sqrt{\frac{k}{\bar{m}}} \quad (2.40)$$

$$\xi = \frac{c}{2\sqrt{\bar{m}k}} \quad (2.41)$$

Here u is the new control input, α is the coupling constant, ω_n is the natural frequency, and ξ is the damping ratio for the flexible appendage.

Chapter III

Review of Controller Design Methods

3.1 Introduction

In this chapter, we first briefly review the relevant control theoretic results that are used in this thesis to design controllers for the flexible appendage system. For full details, the reader is referred to [17], [31], and [36]. The chapter is arranged in the following manner. Section 3.2 summarizes a number of stability concepts. Lyapunov's direct method is described in Section 3.3. The background on notch and IIR filters is included in Section 3.4. Finally, Section 3.5 provides a quick review of the Linear Quadratic Regulator (LQR) method.

3.2 System Stability

Let $\mathbf{x} = (x_1, \dots, x_n)^T$ denote an n dimensional state vector and consider an autonomous nonlinear dynamical system written in the form

$$\dot{\mathbf{x}} = \mathbf{f}(\mathbf{x}) \tag{3.1}$$

where the $\mathbf{f}(\mathbf{x})$ function is considered to be continuously differentiable. Let \mathbf{x}_e denote an equilibrium state, i.e. let

$$\mathbf{f}(\mathbf{x}_e) = 0 \tag{3.2}$$

For simplicity, assume that $\mathbf{x}_e = 0$ (this can always be achieved by shifting the coordinates).

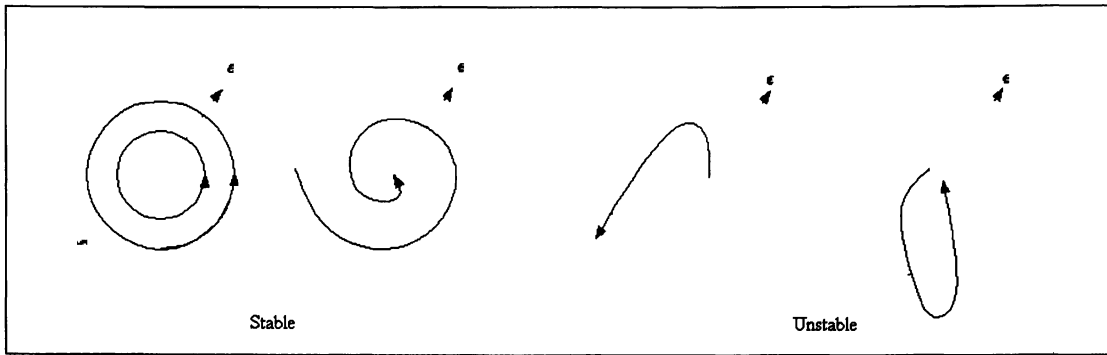


Figure 3.1. Stable and unstable systems.

The equilibrium state is said to be stable if for any $\epsilon > 0$ there exists a $\delta(\epsilon) > 0$ such that

$$\|\mathbf{x}(0)\| < \delta \Rightarrow \|\mathbf{x}(t)\| < \epsilon \quad (3.3)$$

for every $t \geq 0$.

Figure 3.1 shows examples of both stable and unstable systems. The system is considered unstable if it does not satisfy (3.3). For this to occur, there must exist an $\epsilon > 0$ from which no value of δ exists to satisfy the stability requirement.

The system is said to be asymptotically stable if it is stable and δ can be chosen such that

$$\|\mathbf{x}(0)\| < \delta \Rightarrow \lim_{t \rightarrow \infty} \mathbf{x}(t) = 0 \quad (3.4)$$

There are several ways to determine the stability of an equilibrium point, including: solving the differential equation, Lyapunov's first method (also known as the indirect method) as well as Lyapunov's second method (known as the direct method). In this thesis, Lyapunov's direct method is explored further.

3.3 Lyapunov's Direct Method

Proving stability of nonlinear systems with the basic stability definitions and without resorting to local approximations can be quite tedious and difficult. Lyapunov's direct method provides a tool to make rigorous, analytical stability claims of nonlinear systems by studying the behavior of a scalar, energy-like Lyapunov function.

Let $V(\mathbf{x})$ be a continuously differentiable function defined on a domain $D \subset \mathbb{R}^n$, which contains the origin, i.e. the equilibrium state. Then we have the following definitions:

- $V(\mathbf{x})$ is said to be positive definite if $V(0) = 0$ and

$$V(\mathbf{x}) > 0 \quad \forall \mathbf{x} \in D - \{0\} \quad (3.5)$$

- $V(\mathbf{x})$ is positive semidefinite in the same domain if

$$V(\mathbf{x}) \geq 0 \quad \forall \mathbf{x} \in D \quad (3.6)$$

$V(\mathbf{x})$ is said to be negative definite or negative semidefinite if $-V(\mathbf{x})$ is positive definite or is positive semidefinite, respectively.

To determine the stability, both the behavior of both the Lyapunov function and its derivative must be observed. The following results can be stated:

- If $V(\mathbf{x}) > 0$ and $\dot{V}(\mathbf{x}) \leq 0$ in the domain D , then $\mathbf{x} = 0$ is stable.

- If, in addition to the above, $\dot{V}(\mathbf{x})$ is not identically zero along any solution of (3.1) other than the equilibrium in the domain D , then $\mathbf{x} = 0$ is asymptotically stable.

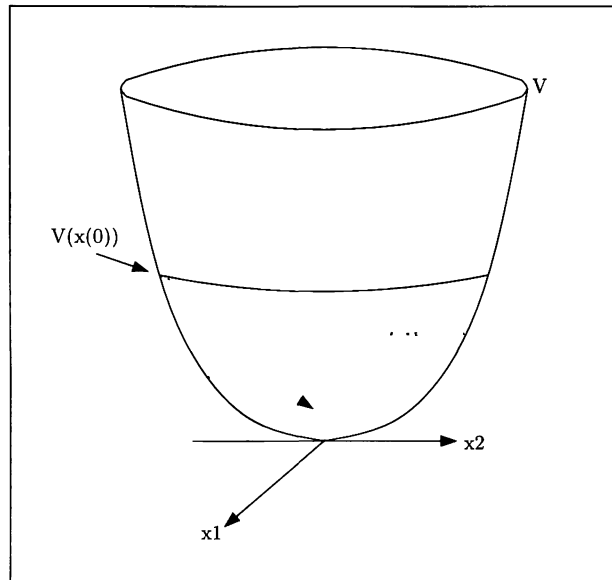


Figure 3.2. Example of a Lyapunov function.

3.4 Filters

Filters are an important component in many controller designs. The purpose of filters in flexible controls is to minimize or remove the effects of vibrational frequencies inherent to the system. Filters can also be used to safeguard the specific mode of the system is not destabilized by feedback control. As stated by B. Wie in [36], filters do not introduce any dampening into the system. To control the rigid body motion, a proportional derivative (PD) controller is utilized. Two different filters are considered in this thesis, a notch filter as well as an IIR filter.

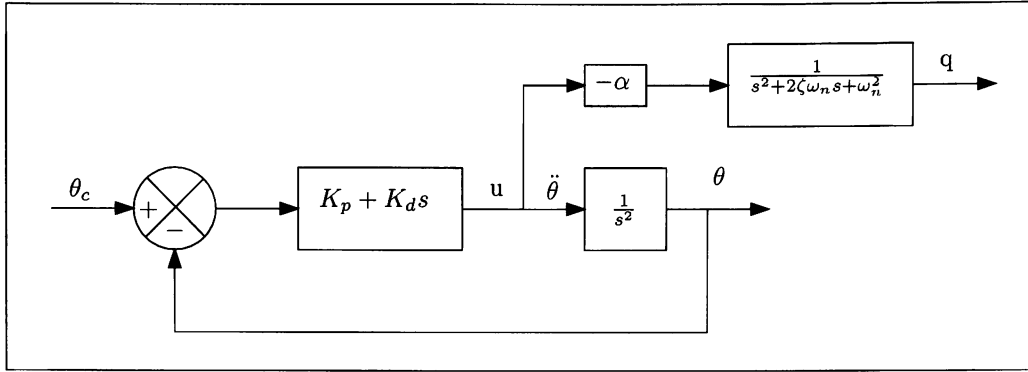


Figure 3.3. Block diagram of a PD controlled system.

3.4.1 Notch Filter

A notch filter, also known as a bandreject filter, is a specialized form of a second-order filter. A generalized format of these filters can be shown as

$$\frac{s^2/\omega_z^2 + 2\xi_z s/\omega_z + 1}{s^2/\omega_p^2 + 2\xi_p s/\omega_p + 1} \quad (3.7)$$

where ω_z , ω_p , ξ_z , and ξ_p are filter parameters. Different choices and combinations for these parameters yield different filter designs such as lead/lag and all pass filters as well as the notch filter. For the notch filter design for the system in the paper, the parameters are chosen as $\omega_n = \omega_z = \omega_p$.

The filter dampening ratios for a notch filter are defined as

$$\xi_z = 0 \text{ and } \xi_p = 1$$

Making these substitutions into the original generalized format yields

$$\frac{s^2/\omega_n^2 + 1}{s^2/\omega_n^2 + 2s/\omega_n + 1} \quad (3.8)$$

which simplifies to the general notch filter

$$\frac{s^2 + \omega_n^2}{(s + \omega_n)^2} \quad (3.9)$$

The block diagram representing a notch filter applied to a PD controlled system is shown in Figure 3.4.

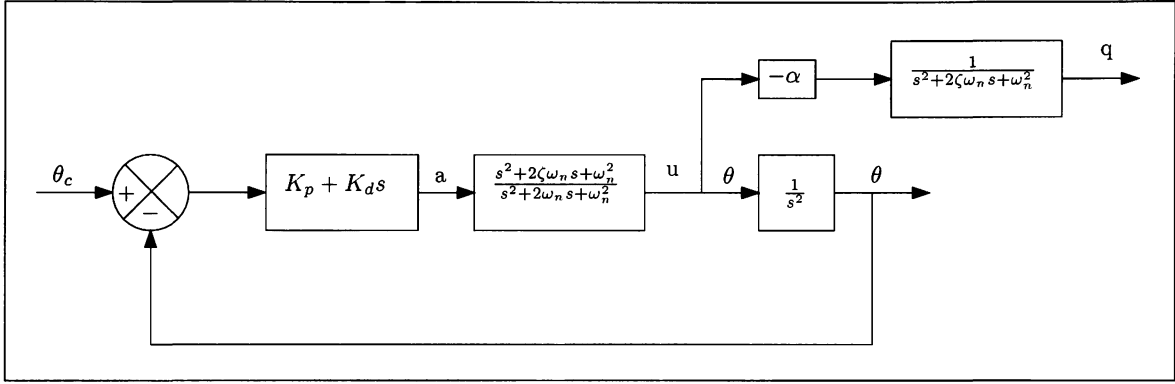


Figure 3.4. Block diagram of notch filter applied to a PD controlled system.

3.4.2 IIR Filter

The Infinite Impulse Response (IIR) filter is another filter that can be used to reduce the effects of vibrational modes. The continuous s-domain representation of an IIR filter is given by

$$\frac{\delta^3}{\omega_n^2} \left(\frac{s^2 + 2\xi\omega_n s + \omega_n^2}{(s + \delta)^3} \right) \quad (3.10)$$

The initial setup of the filter is similar to that of the notch filter, with the addition of a time constant δ . The result of applying this filter to an underdamped second order system, like the system used in this thesis, is a third order critically damped system. The

filter cancels underdamped poles from the second order equation and replaces them with the critically damped third order poles.

The block diagram representing an IIR filter applied to a PD controlled system is shown in Figure 3.5.

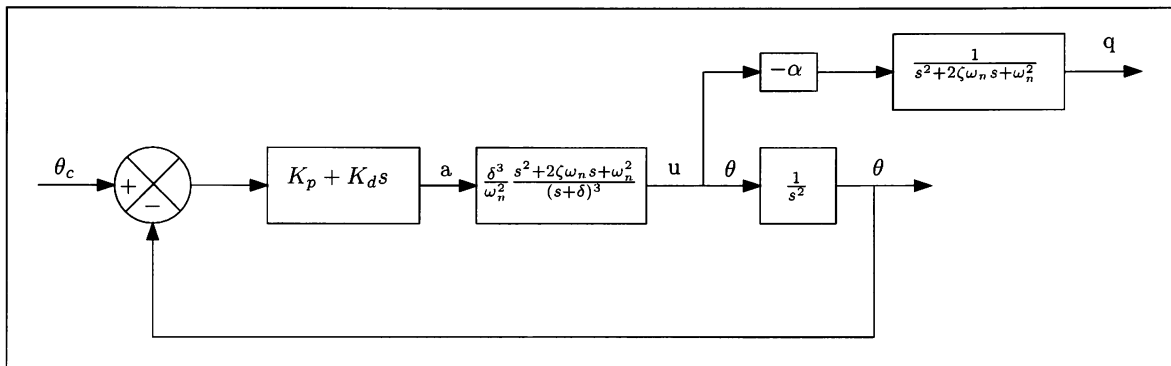


Figure 3.5. IIR filter applied to a PD controlled system.

3.5 Linear Quadratic Regulator

The linear quadratic regulator method provides a way to compute the state feedback control gain matrix for a system. We start with a single input linear time-invariant system

$$\dot{x} = Ax + Bu \quad (3.11)$$

where x and u are the state space and input variables for the system. LQR method is employed to determine the optimal feedback control

$$u = -Kx \quad (3.12)$$

that minimizes the cost function

$$J(u) = \int_0^{\infty} (\mathbf{x}^T \mathbf{Q} \mathbf{x} + u^T \mathbf{R} u) dt \quad (3.13)$$

This thesis utilizes the MATLAB built-in function *lqr()* to solve for the optimal gain \mathbf{K} for the system.

Chapter IV

Controller Design

4.1 Introduction

In this chapter, we develop and apply four different controller designs for the system. It is demonstrated that PD feedback can be combined with a Notch filter or an IIR (Infinite Impulse Response) filter to insure that the inputs at the vibration frequencies are not passed through the filter. Finally, the Lyapunov method is applied to design nonlinear controllers.

4.2 A PD Controller with Notch Filter

Consider the block diagram in Figure 3.4. The linearized equations can be written as

$$\ddot{\theta} = u \quad (4.1)$$

$$\ddot{q} + 2\zeta\omega_n\dot{q} + \omega_n^2 q = -\alpha u \quad (4.2)$$

The output of the PD controller is given by (with $\theta_c = 0$ as the equilibrium point)

$$a = -K_p\theta - K_d\dot{\theta} \quad (4.3)$$

where K_p and K_d represent the controller gains. The notch filter can be expressed as a transfer function from the input a to the output u of the filter as

$$\frac{u}{a} = \frac{s^2 + 2\xi\omega_n s + \omega_n^2}{(s + \omega_n)^2} \quad (4.4)$$

or, equivalently, as

$$\ddot{u} + 2\omega_n\dot{u} + \omega_n^2 u = \ddot{a} + 2\xi\omega_n\dot{a} + \omega_n^2 a \quad (4.5)$$

To obtain a state-space realization of the filter define an auxiliary signal z satisfying

$$\ddot{z} + 2\omega_n \dot{z} + \omega_n^2 z = a \quad (4.6)$$

so that the transfer function from a to z is given by

$$\frac{z}{a} = \frac{1}{s^2 + 2\omega_n s + \omega_n^2} \quad (4.7)$$

Clearly, the filter output can be expressed as

$$u = \ddot{z} + 2\xi\omega_n \dot{z} + \omega_n^2 z \quad (4.8)$$

Substituting \ddot{z} from equation (4.6) simplifies to

$$u = a - 2\omega_n(1 - \xi)\dot{z} \quad (4.9)$$

thus yielding a new equation for the output of the filter.

Define the state variables

$$(x_1, x_2, x_3, x_4, x_5, x_6) = (\theta, \dot{\theta}, q, \dot{q}, z, \dot{z})$$

so that the closed-loop system (including the nonlinearity $\dot{\theta}^2 q$) can be written as:

$$\dot{x}_1 = x_2 \quad (4.10)$$

$$\dot{x}_2 = u \quad (4.11)$$

$$\dot{x}_3 = x_4 \quad (4.12)$$

$$\dot{x}_4 = -\omega_n^2 x_3 - 2\xi\omega_n x_4 - \alpha u + x_2^2 x_3 \quad (4.13)$$

$$\dot{x}_5 = x_6 \quad (4.14)$$

$$\dot{x}_6 = -2\omega_n x_6 - \omega_n^2 x_5 + a \quad (4.15)$$

where

$$a = -K_p x_1 - K_d x_2 \quad (4.16)$$

$$u = a - 2\omega_n(1 - \xi)x_6 \quad (4.17)$$

4.3 A PD Controller with IIR Filter

The Infinite Impulse Response (IIR) filter is another filter that is applied to this control problem. Consider again the linearized system

$$\ddot{\theta} = u \quad (4.18)$$

$$\ddot{q} + 2\zeta\omega_n\dot{q} + \omega_n^2q = -\alpha u \quad (4.19)$$

The IIR filter can be expressed as a transfer function from the input a to the output u of the filter as

$$\frac{u}{a} = \frac{\delta^3}{\omega_n^2} \left(\frac{s^2 + 2\zeta\omega_n s + \omega_n^2}{(s + \delta)^3} \right) \quad (4.20)$$

where δ is the time constant for the filter. To obtain a state-space realization of the filter define an auxiliary signal z satisfying

$$\ddot{z} + 3\delta\dot{z} + 3\delta^2z + \delta^3z = \frac{\delta^3}{\omega_n^2} a \quad (4.21)$$

Clearly, the filter output can be expressed as

$$u = \ddot{z} + 2\zeta\omega_n\dot{z} + \omega_n^2z \quad (4.22)$$

Define the state variables

$$(x_1, x_2, x_3, x_4, x_5, x_6, x_7) = (\theta, \dot{\theta}, q, \dot{q}, z, \dot{z}, \ddot{z})$$

so that the closed-loop system (including the nonlinearity $\dot{\theta}^2 q$) can be written as:

$$\dot{x}_1 = x_2 \quad (4.23)$$

$$\dot{x}_2 = u \quad (4.24)$$

$$\dot{x}_3 = x_4 \quad (4.25)$$

$$\dot{x}_4 = -\omega_n^2 x_3 - 2\xi\omega_n x_4 - \alpha u + x_3 x_2^2 \quad (4.26)$$

$$\dot{x}_5 = x_6 \quad (4.27)$$

$$\dot{x}_6 = x_7 \quad (4.28)$$

$$\dot{x}_7 = \frac{\delta^3}{\omega_n^2} a - \delta^3 x_5 - 3\delta^2 x_6 - 3\delta x_7 \quad (4.29)$$

where

$$a = -K_p x_1 - K_d x_2 \quad (4.30)$$

$$u = x_7 + 2\omega_n \xi x_6 + \omega_n^2 x_5 \quad (4.31)$$

4.4 LQR

LQR method is applied in the following manner. From (2.17)-(2.18) the linearized system can be written as

$$\dot{x} = Ax + Bu$$

where $x = (\theta, \dot{\theta}, q, \dot{q})^T$ is the state vector, u the control input, and

$$A = \begin{bmatrix} 0 & 1 & 0 & 0 \\ 0 & 0 & 0 & 0 \\ 0 & 0 & 0 & 1 \\ 0 & 0 & -\omega_n^2 & -2\xi\omega_n \end{bmatrix} \quad (4.32)$$

$$B = \begin{bmatrix} 0 \\ 1 \\ 0 \\ -\alpha \end{bmatrix} \quad (4.33)$$

It should also be noted that the nonlinear term is ignored prior to application of the LQR method.

Next, the weighting matrices \mathbf{Q} and \mathbf{R} are chosen for the system. \mathbf{Q} can be either a positive definite or a positive semidefinite matrix whereas \mathbf{R} must be a positive definite matrix. They should be chosen to minimize the cost index equation when applied to the state space variables. Generally, diagonal matrices, including the identity matrix, are utilized for \mathbf{Q} and \mathbf{R} .

Utilizing the built-in function *lqr* in MATLAB, the optimal gain \mathbf{K} is determined such that the cost function

$$J(u) = \int_0^{\infty} (\mathbf{x}^T \mathbf{Q} \mathbf{x} + u^T \mathbf{R} u) dt \quad (4.34)$$

is minimized. The optimal linear feedback is then given by

$$u = -\mathbf{K} \mathbf{x} \quad (4.35)$$

and the state matrix for the controlled system becomes

$$\mathbf{A}_{new} = \mathbf{A} - \mathbf{B} \mathbf{K} \quad (4.36)$$

4.5 Lyapunov-Based Design

Again recall the nonlinear system dynamics described as

$$\ddot{\theta} = u \quad (4.37)$$

$$\ddot{q} + 2\xi\omega_n\dot{q} + \omega_n^2 q = -\alpha u + q\dot{\theta}^2 \quad (4.38)$$

Let $\mathbf{x} = (\theta, \dot{\theta}, q, \dot{q})^T$ and consider a Lyapunov function candidate given by

$$V = \frac{K_1}{2}\theta^2 + a\frac{\dot{\theta}^2}{2} + \frac{b}{2}\dot{q}^2 + \frac{b\omega_n^2}{2}q^2 + \alpha b\dot{q}\dot{\theta} \quad (4.39)$$

Clearly, V is positive definite if $K_1 > 0, a > 0, b > 0, a - \alpha^2 b > 0$. For asymptotic stability, it suffices to show that $\dot{V} \leq 0$ and \dot{V} is not identically zero along any solution of (4.37)-(4.38) other than the equilibrium $\mathbf{x} = 0$.

The time rate of change for the Lyapunov function candidate along the trajectories of (4.37)-(4.38) can be computed as

$$\dot{V} = -2b\xi\omega_n\dot{q}^2 + \dot{\theta} \left[K_1\theta + au + bq\dot{q}\dot{\theta} + \alpha b(-2\xi\omega_n\dot{q} - \omega_n^2 q - \alpha u + \dot{\theta}^2 q) \right] \quad (4.40)$$

It is easily seen that the first term will always satisfy the requirements for asymptotic stability, so a new term is introduced into the function to insure that it will always remain less than zero for AS. Choosing

$$-K_2\dot{\theta} = (a - \alpha^2 b)u + K_1\theta + bq\dot{q}\dot{\theta} - 2\alpha b\xi\omega_n\dot{q} - \alpha b\omega_n^2 q + \alpha b\dot{\theta}^2 q \quad (4.41)$$

yields

$$\dot{V} = -2b\xi\omega_n\dot{q}^2 - K_2\dot{\theta}^2 \quad (4.42)$$

which satisfies $\dot{V} \leq 0$. Note that $\dot{V} \equiv 0 \Rightarrow (\dot{\theta} \equiv 0, \dot{q} \equiv 0) \Rightarrow x = 0$, i.e. \dot{V} is not identically zero along any solution of (4.19)-(4.20) other than the equilibrium $x = 0$.

From the substitution above, the input u is defined as follows

$$u = \frac{-K_2 \dot{\theta} - K_1 \theta - bq\dot{q}\dot{\theta} + 2\alpha b\xi\omega_n \dot{q} + \alpha b\omega_n^2 q - \alpha b\dot{\theta}^2 q}{a - \alpha^2 b} \quad (4.43)$$

Define the state variables

$$(x_1, x_2, x_3, x_4) = (\theta, \dot{\theta}, q, \dot{q})$$

so that the closed-loop system can be written as:

$$\dot{x}_1 = x_2 \quad (4.44)$$

$$\dot{x}_2 = u \quad (4.45)$$

$$\dot{x}_3 = x_4 \quad (4.46)$$

$$\dot{x}_4 = -\omega_n^2 x_3 - 2\xi\omega_n x_4 - \alpha u + x_3 x_2^2 \quad (4.47)$$

where

$$u = \frac{-K_2 x_2 - K_1 x_1 - bx_2 x_3 x_4 + 2\alpha b\xi\omega_n x_4 + \alpha b\omega_n^2 x_3 - \alpha bx_2^2 x_3}{a - \alpha^2 b} \quad (4.48)$$

Chapter V

Experimental Setup

5.1 Introduction

This section of the thesis will utilize the control methods that have been described and apply them to a known experimental setup. The proposed setup is composed of several components. The two main components that will be used in the modeling process for this thesis include the *Rotary Flexible Link module (FLEXGAGE)* and the *SRV02* plant produced by Quanser shown in Figure 5.1. This setup is comprised of a thin stainless steel link as the flexible appendage as well as a servomotor. Further research will use this flexible link module to demonstrate the effectiveness of the controllers designed in this thesis.

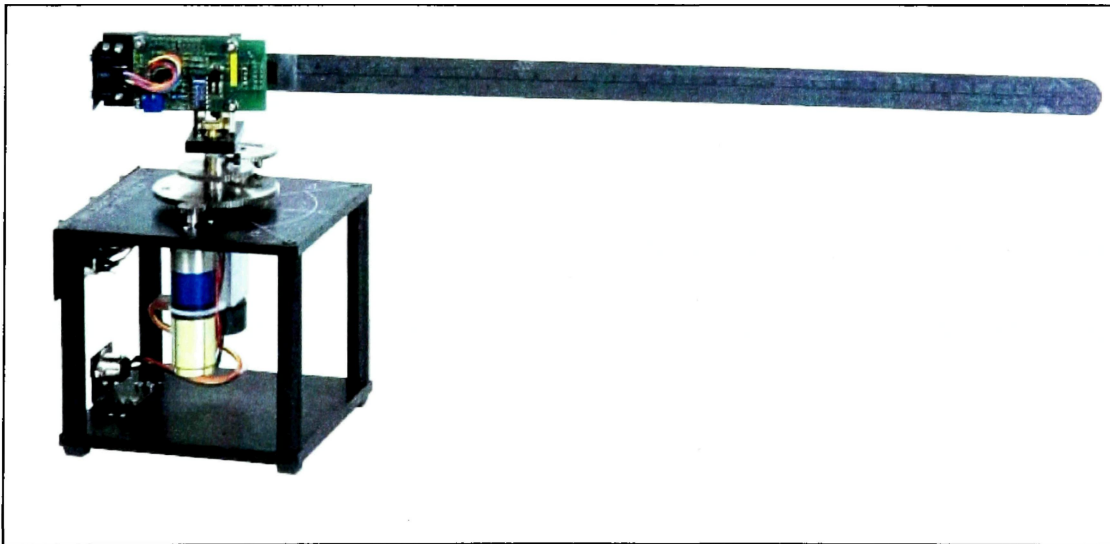


Figure 5.1. The flexible link module setup. (Quanser.com)

To properly generate the torque profile developed by the controllers, the input voltage to the motor must be derived to dampen the vibrations caused by an attitude change in the system. This modeling of setup will ignore any affects caused by air resistance as well as the effect of gravity. The gravitational influence is ignored with the understanding that the plane of motion of the setup is perpendicular to the force of gravity caused by the Earth.

The next two sections will introduce the system dynamics of the motor as well as the controllers being applied to the system. Section 5.2 will go through the formulation of the mathematical model for the Quanser motor setup. The application of the controllers designed in the previous sections will be shown in Section 5.3.

5.2 Mathematical Model of Actuator Dynamics

The torque developed by the motor is

$$T_m = \eta_m \eta_g K_t I_a \quad (5.1)$$

where K_t is the motor torque constant and I_a is the armature current. The motor and gearbox efficiencies are represented by η_m and η_g , respectively. The differential equation for the armature circuit is then given by

$$L_a \dot{I}_a + R_a I_a + E_m = V_i \quad (5.2)$$

where V_i is the armature voltage (input to the servomotor), L_a is the armature inductance, R_a is the armature resistance, and E_m is the back electromotive force (EMF) voltage of the motor.

The back EMF of the motor is defined as follows

$$E_m = K_m \dot{\theta}_m \quad (5.3)$$

where K_m is the motor voltage constant and $\dot{\theta}_m$ is the angular velocity of the motor. The angular velocity of the motor can also be represented in terms of the gear ratio K_g and the angular velocity of the system $\dot{\theta}$ as

$$\dot{\theta}_m = K_g \dot{\theta} \quad (5.4)$$

where the system torque is

$$\tau = K_g T_m \quad (5.5)$$

Substituting these values and solving (5.2) using (5.1) yields

$$L_a \dot{I}_a + \frac{R_a}{\eta_m \eta_g K_t K_g} \tau = V_i - K_m K_g \dot{\theta} \quad (5.6)$$

In general, the armature inductance L_a is very small ($L_a \approx 0$) and is therefore ignored in this thesis. Consequently, (5.6) simplifies to

$$\frac{R_a}{\eta_m \eta_g K_t K_g} \tau = V_i - K_m K_g \dot{\theta} \quad (5.7)$$

Solving for system torque τ yields

$$\tau = \frac{\eta_m \eta_g K_t K_g}{R_a} (V_i - K_m K_g \dot{\theta}) \quad (5.8)$$

This is the same torque that is derived from the partial feedback equations. The calculation from the controller can be substituted for τ to solve for the voltage output, V_i , of the motor for the system

$$V_i = \frac{R_a}{\eta_m \eta_g K_t K_g} \tau + K_m K_g \dot{\theta} \quad (5.9)$$

5.3 Physical Values for the Experimental Setup

We apply the controllers designed previously to the Quanser flexible link experiment module. The distributed parameter model will be utilized for the experimental simulations for the system.

Table 5.1. Flexible arm parameters

Variable	Name	Value	Units
l_0	Distance attach pt. to center of rotation	~ 0	m
l	Length of arm	0.483	m
m	Mass of beam	0.065	kg
ρ_l	Beam mass per unit length	0.1346	kg/m
E	Modulus of elasticity of beam	7.1×10^{10}	N/m ²
I	Beam area moment of inertia	4.125×10^{-12}	m ⁴
EI	Beam uniform flexural rigidity	0.293	N·m ²
k	Stiffness coefficient	379.77	N·m/rad
c	Mechanical dissipative constant	0.0339	N·m/rad/s
ξ	Damping ratio of beam	0.001	N/A

Table 5.2. Servo motor parameters

Variable	Name	Value	Units
R_a	Armature resistance	2.6	Ω
L_a	Armature inductance	0.18	mH
η_m	Motor efficiency	0.69	N/A
η_g	Gearbox efficiency	0.85	N/A
K_t	Motor torque constant	0.00767	N·m
K_m	Motor voltage/back EMF constant	0.00767	V/rad/s
K_g	Gear ratio	60:1	N/A
I_z	Equivalent mass moment of inertia	188.84×10^{-5}	$\text{kg}\cdot\text{m}^2$
V_{\max}	Input Voltage range	± 10	V

Recalling the equations of motion for the distributed parameter model (2.15) and (2.16)

$$\left[I_t + m_q q^2 \right] \ddot{\theta} + m_{\theta q} \ddot{q} + 2m_q q \dot{q} \dot{\theta} = \tau$$

$$m_q \ddot{q} + m_{\theta q} \ddot{\theta} - m_q q \dot{\theta}^2 + kq + c\dot{q} = 0$$

The physical values are then applied to the system. The $m_{\theta q}$, m_q and k terms are computed through integration by parts to be

$$m_{\theta q} = \rho_l l^2 \left(\frac{1}{2} + \frac{2}{\pi^2} + \frac{\pi^2}{8} \right) = .0608 \text{ kg}\cdot\text{m}$$

$$m_q = \rho_l l \left(1 + 2 + \frac{1}{2} + \frac{\pi}{3} + \frac{\pi^4}{20} \right) = 0.758 \text{ kg}$$

$$k = EI \left(1 + \frac{1}{2} \right) \frac{\pi^4}{l^3} = 379.94 \text{ N/m}$$

Through substitution from the partial feedback linearized model,

$$\omega_n = \sqrt{\frac{k}{m_q}} = 22.38 \text{ rad/s}$$

Noting that $\xi = 0.001$, c is then solved as

$$c = 2m_q \xi \omega_n = 0.033 \text{ N}\cdot\text{s/m}$$

The coupling constant, α becomes

$$\alpha = \frac{m_{\theta q}}{m_q} = 0.086 \text{ m}$$

Substituting these values into the original equations of motion yields

$$(0.0069 + 0.758q^2)\ddot{\theta} + 0.0608\dot{q} + 1.516q\dot{q}\dot{\theta} = \tau$$

$$\ddot{q} + 0.045\dot{q} + 501.08q = -0.0802\ddot{\theta} + q\dot{\theta}^2$$

and solving for the torque of the system we obtain

$$\tau = (0.002 + 0.758q^2)u + 1.516q\dot{q}\dot{\theta} - 0.0027\dot{q} - 30.57q + 0.061q\dot{\theta}^2$$

The voltage required by the motor to produce the torque then becomes in terms of the torque τ :

$$V_i = 9.63\tau + 0.46\dot{\theta}$$

or in terms of the state space variables

$$V_i = (0.019 + 7.30q^2)u + 11.10q\dot{q}\dot{\theta} - 0.026\dot{q} - 294.48q + 0.59q\dot{\theta}^2 + 0.46\dot{\theta}$$

5.4 Application of Control Methods

Two separate test cases are applied to the experimental setup using the methods derived in this thesis. The initial values for each of the test cases are shown in Table 5.3.

Table 5.3. Initial conditions for test cases.

	Attitude change	Other ICs
Case 1	$\theta_0 = 0.5 \text{ rad}$	0
Case 2	$\theta_0 = \pi \text{ rad}$	$\dot{\theta}_0 = 0.1 \text{ rad/s}$

For both of the cases, the initial values for $q, \dot{q}, z, \dot{z}, \ddot{z}$ are all set equal to zero. Each of the test cases were applied to the following 4 control designs: PD controller with notch filter, PD controller with IIR filter, LQR controller, and the Lyapunov-based controller. Simulations were done using the MATLAB function ode45.

The controller parameters were chosen as follows (applied for both cases)

Table 5.4. Controller parameters.

PD with Notch Filter: equations (4.10)-(4.17)	
$K_p = 5$	
$K_d = 12$	
PD with IIR Filter: equations (4.23)-(4.31)	
$K_p = 11$	$\delta = 30$
$K_d = 10$	
LQR: equations (4.32)-(4.33), (4.35)	
$Q = \begin{bmatrix} .05 & 0 & 0 & 0 \\ 0 & 40 & 0 & 0 \\ 0 & 0 & 0.01 & 0 \\ 0 & 0 & 0 & 40 \end{bmatrix}, \quad R = [1]$	
$K = [0.224 \quad 6.36 \quad -35.2 \quad -5.55]$	
$\sigma(A_{new}) = \{-6.33, -0.035, -0.245 + 22.4i, -0.245 - 22.4i\}$	
Lyapunov: equations (4.44)-(4.48)	
$K_1 = 0.1$	$a = 1.45$
$K_2 = 3$	$b = 70$

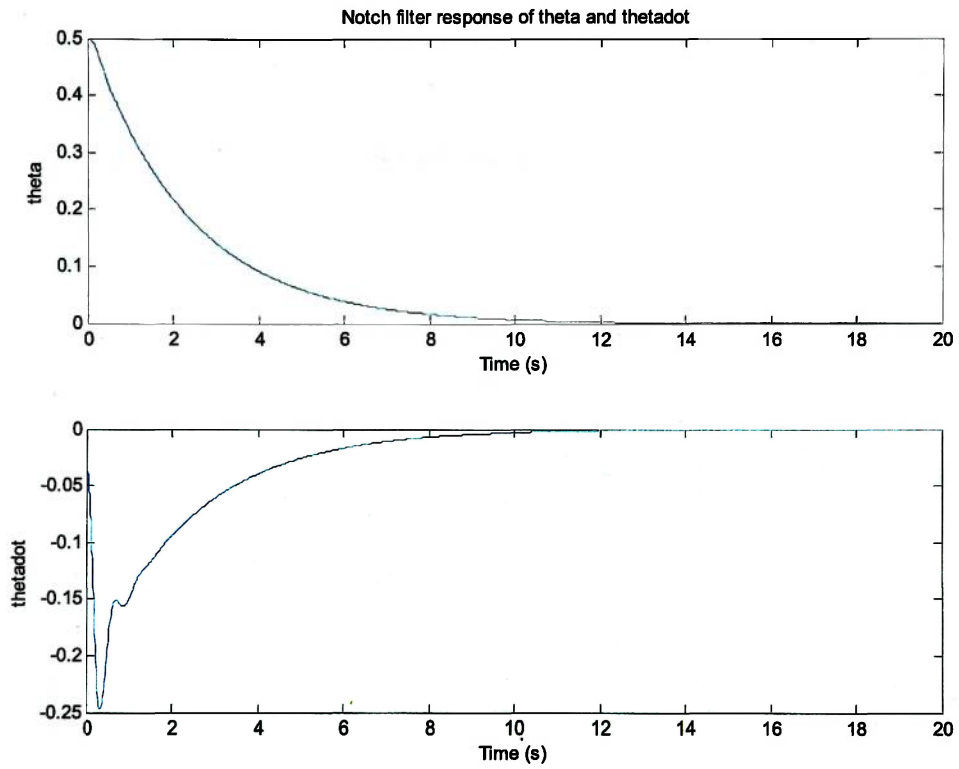


Figure 5.2. Case 1 PD Control with Notch filter θ and $\dot{\theta}$ responses.

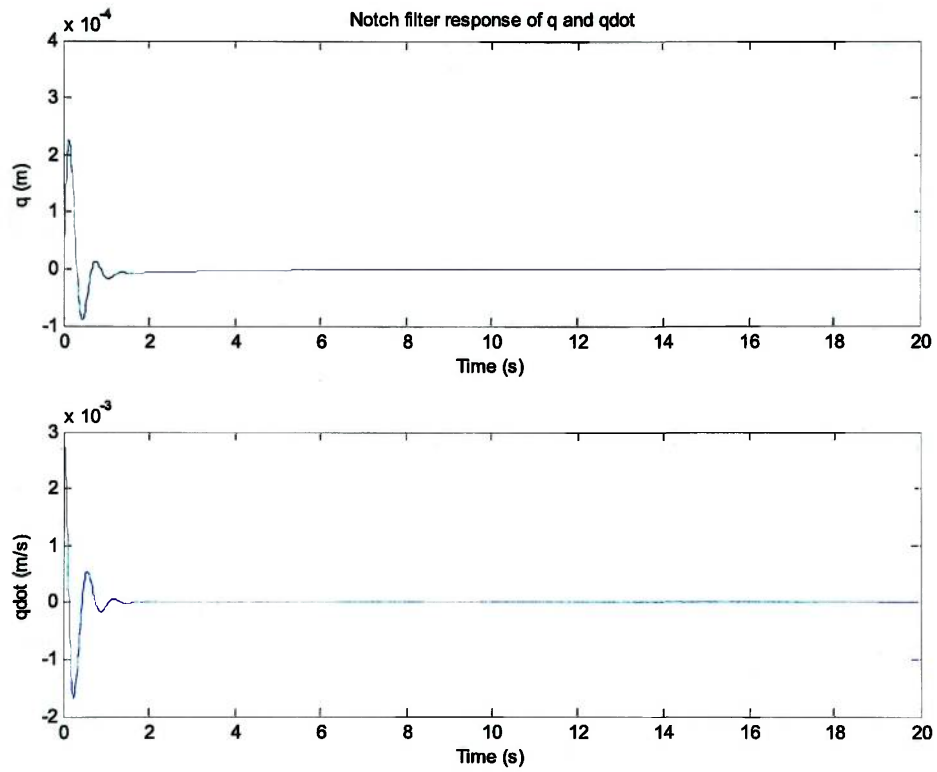


Figure 5.3. Case 1 PD Control with Notch filter q and \dot{q} responses.

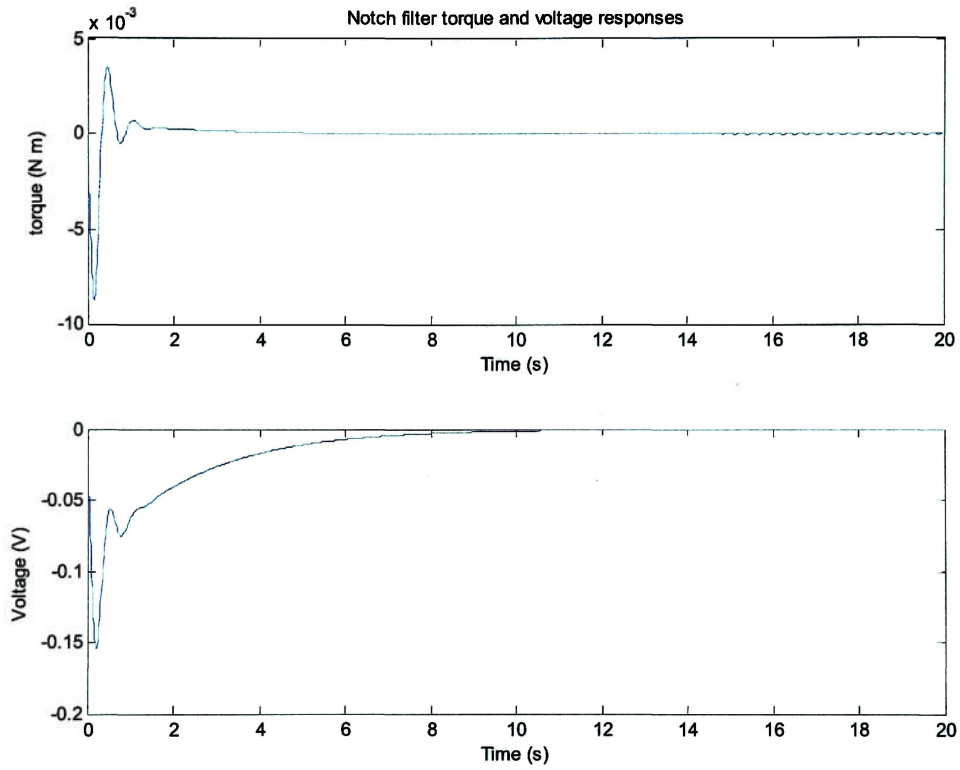


Figure 5.4. Case 1 PD Control with Notch filter τ and V_i responses.

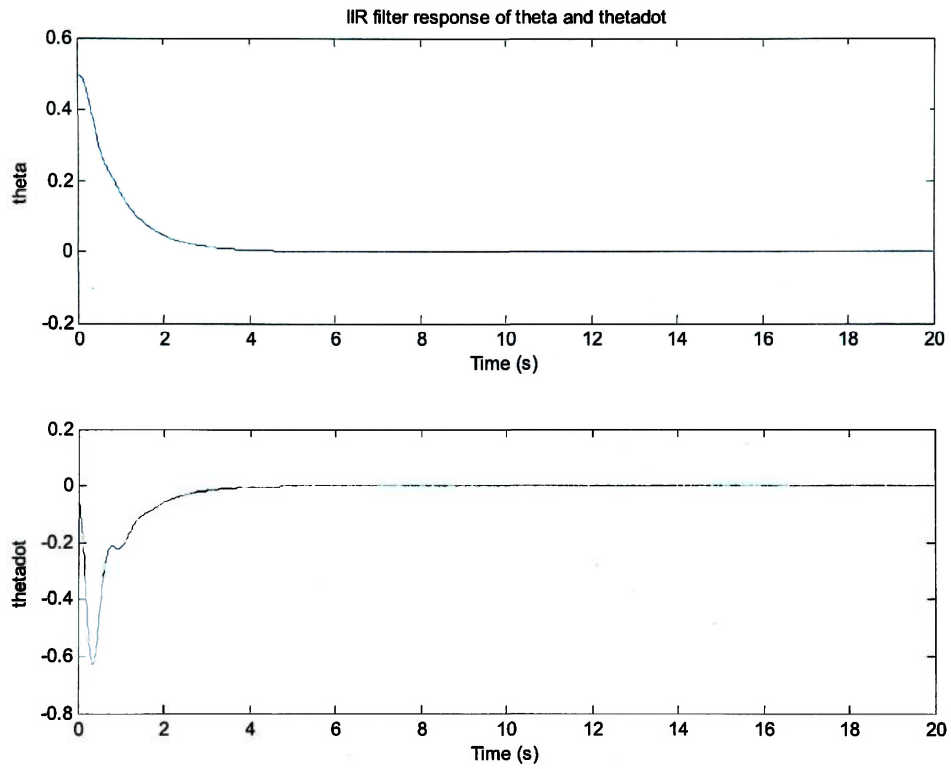


Figure 5.5. Case 1 PD Control with IIR filter θ and $\dot{\theta}$ responses.

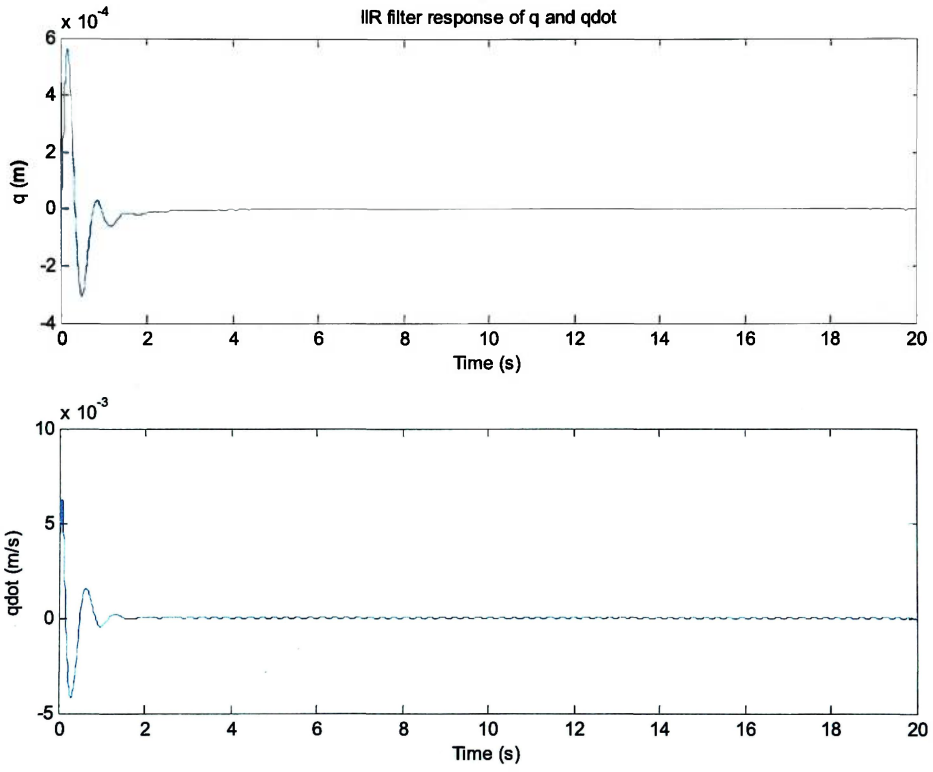


Figure 5.6. Case 1 PD Control with IIR filter q and \dot{q} responses.

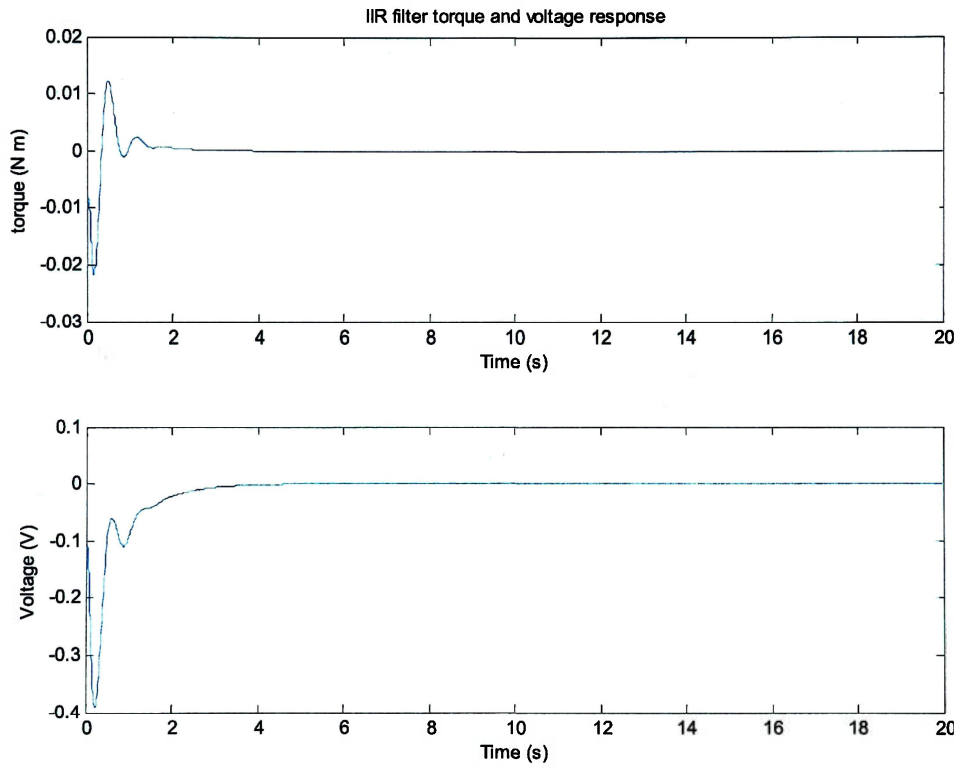


Figure 5.7. Case 1 PD Control with IIR filter τ and V_i responses.

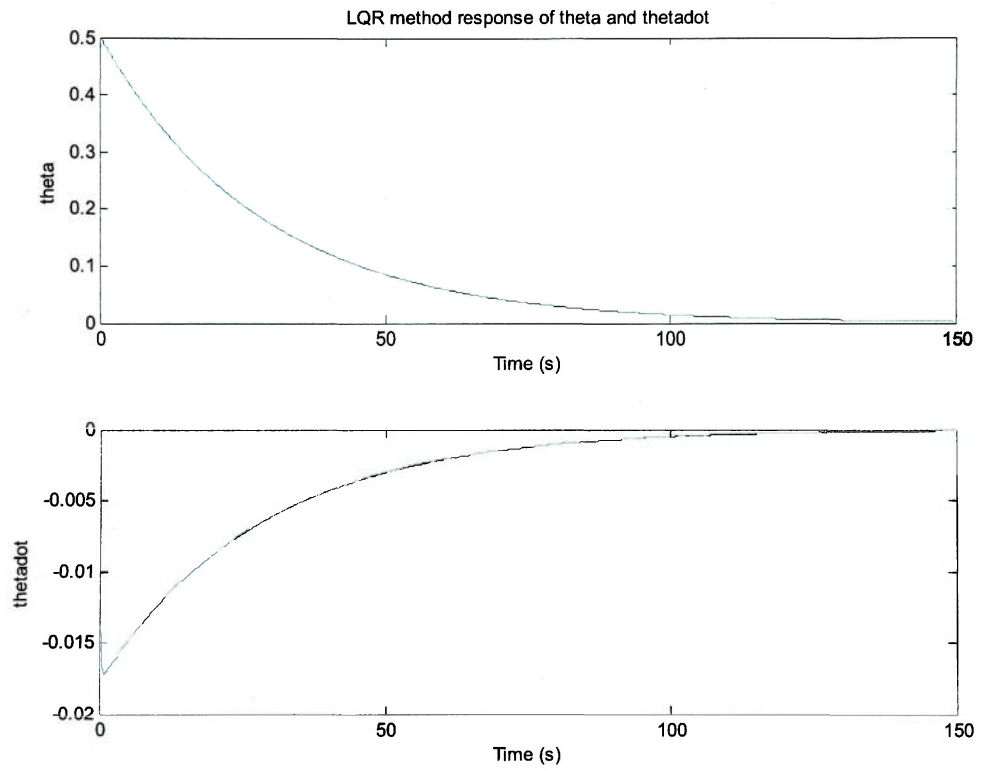


Figure 5.8. Case 1 LQR method θ and $\dot{\theta}$ responses.

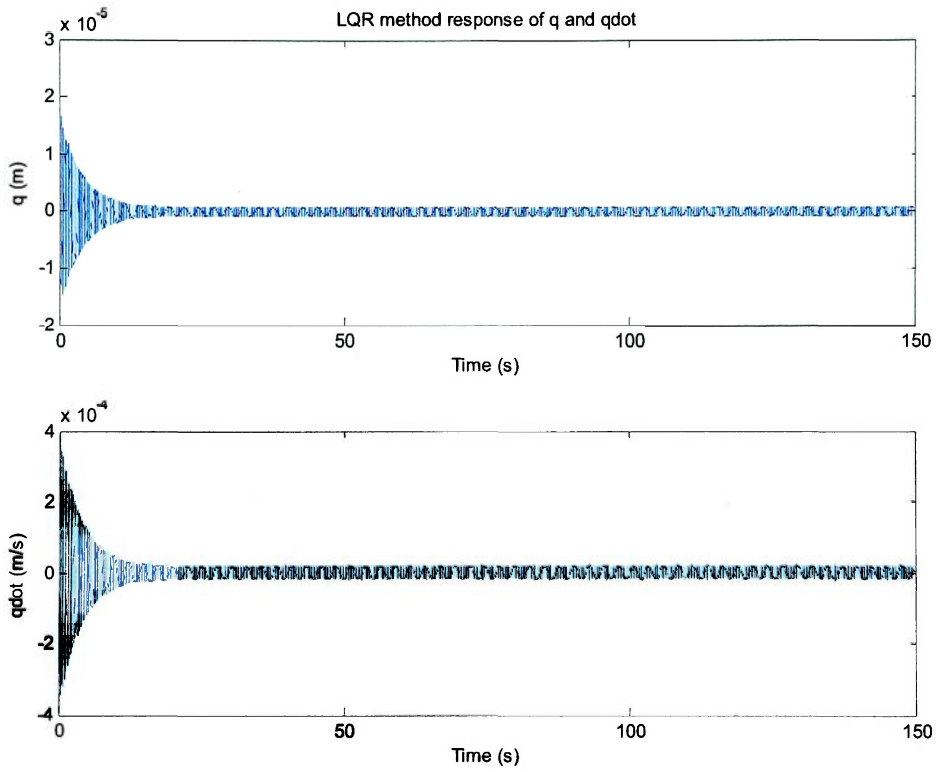


Figure 5.9. Case 1 LQR method q and \dot{q} responses.

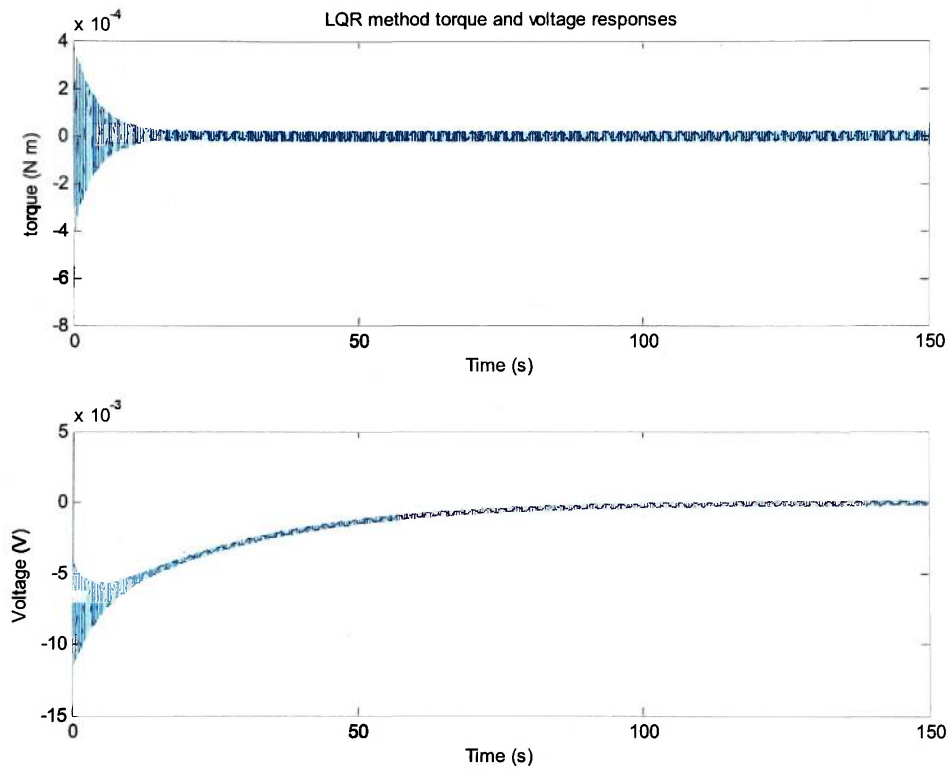


Figure 5.10. Case 1 LQR method τ and V_i responses.

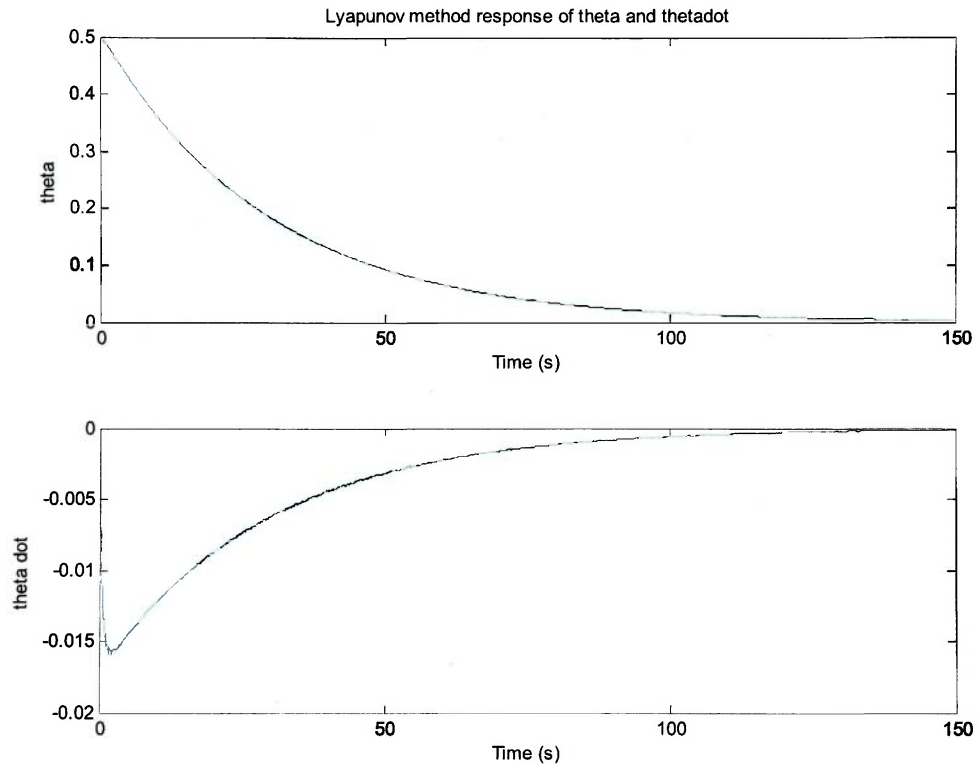


Figure 5.11. Case 1 Lyapunov method θ and $\dot{\theta}$ responses.

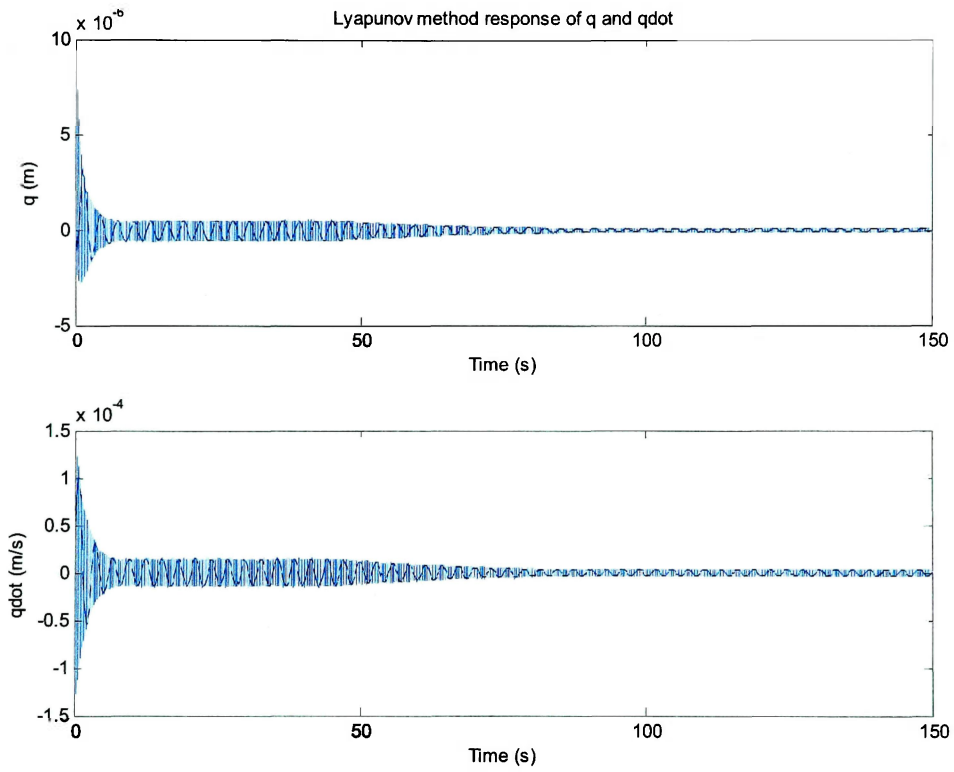


Figure 5.12. Case 1 Lyapunov method q and \dot{q} responses.

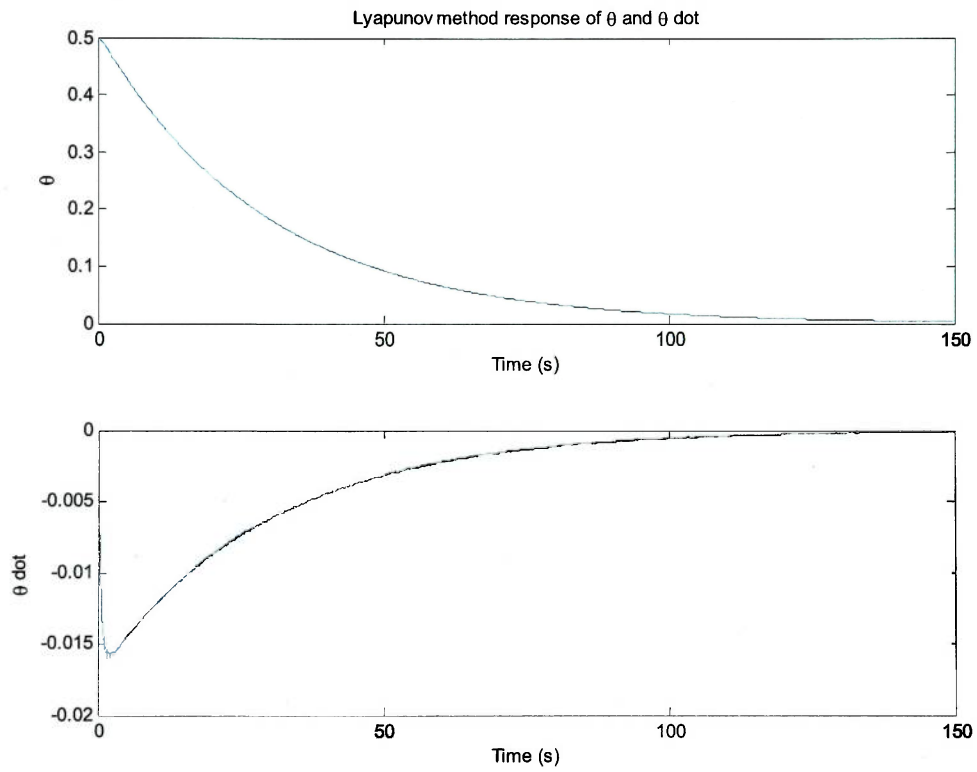


Figure 5.13. Case 1 Lyapunov method τ and V_i responses.

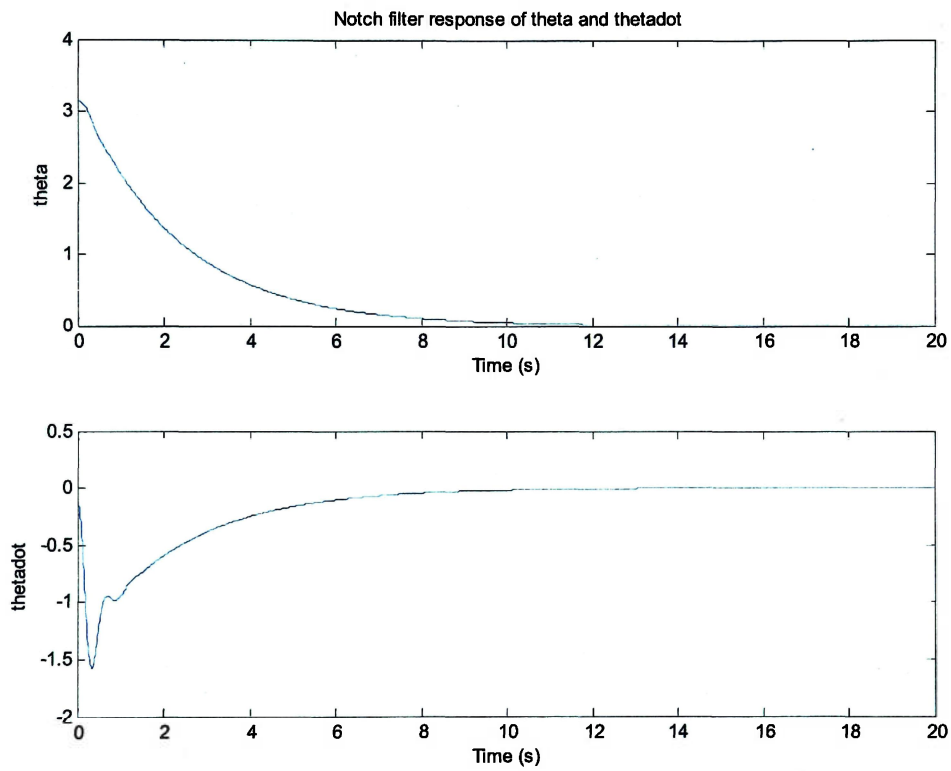


Figure 5.14. Case 2 PD Control with Notch filter θ and $\dot{\theta}$ responses.

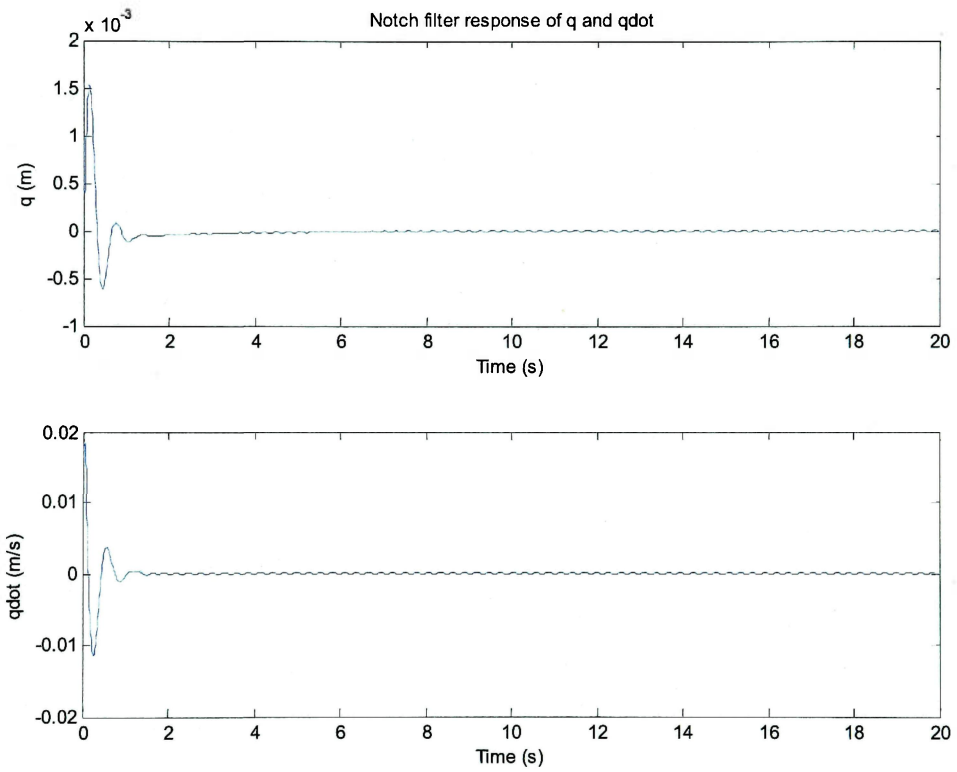


Figure 5.15. Case 2 PD Control with Notch filter q and \dot{q} responses.

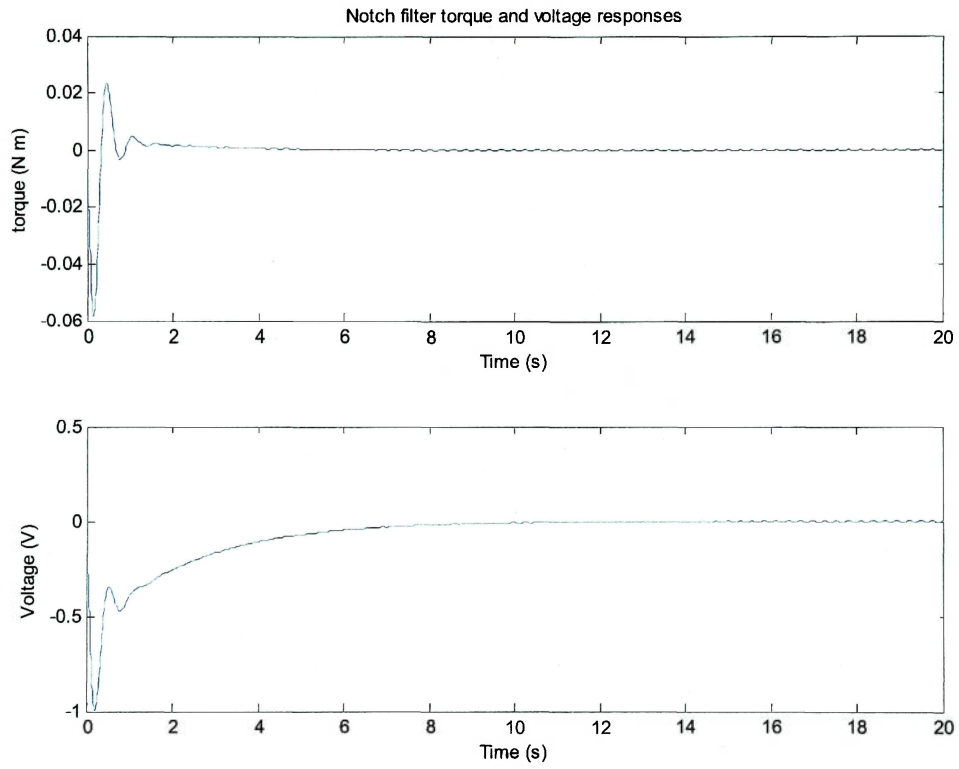


Figure 5.16. Case 2 PD Control with Notch filter τ and V_i responses.

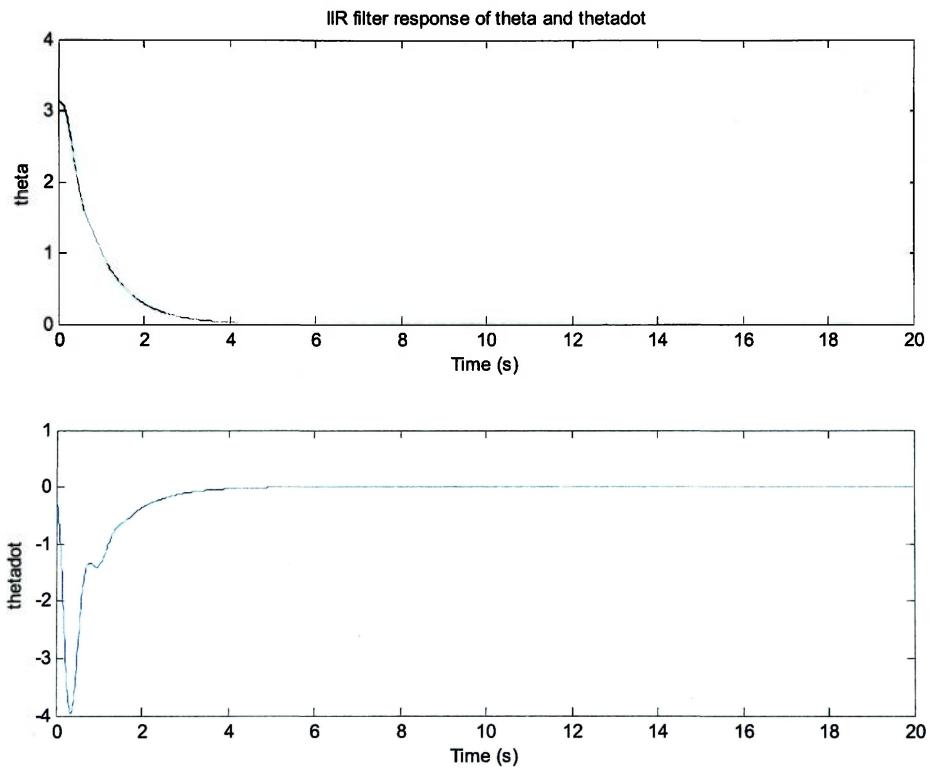


Figure 5.17. Case 2 PD Control with IIR filter θ and $\dot{\theta}$ responses.

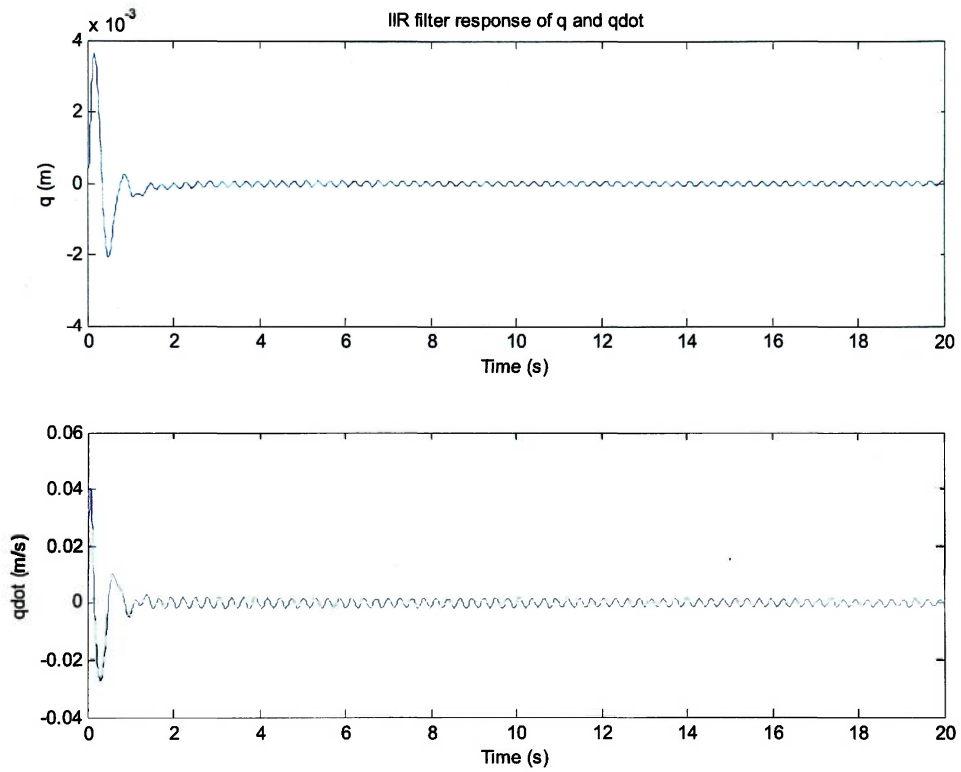


Figure 5.18. Case 2 PD Control with IIR filter q and \dot{q} responses.

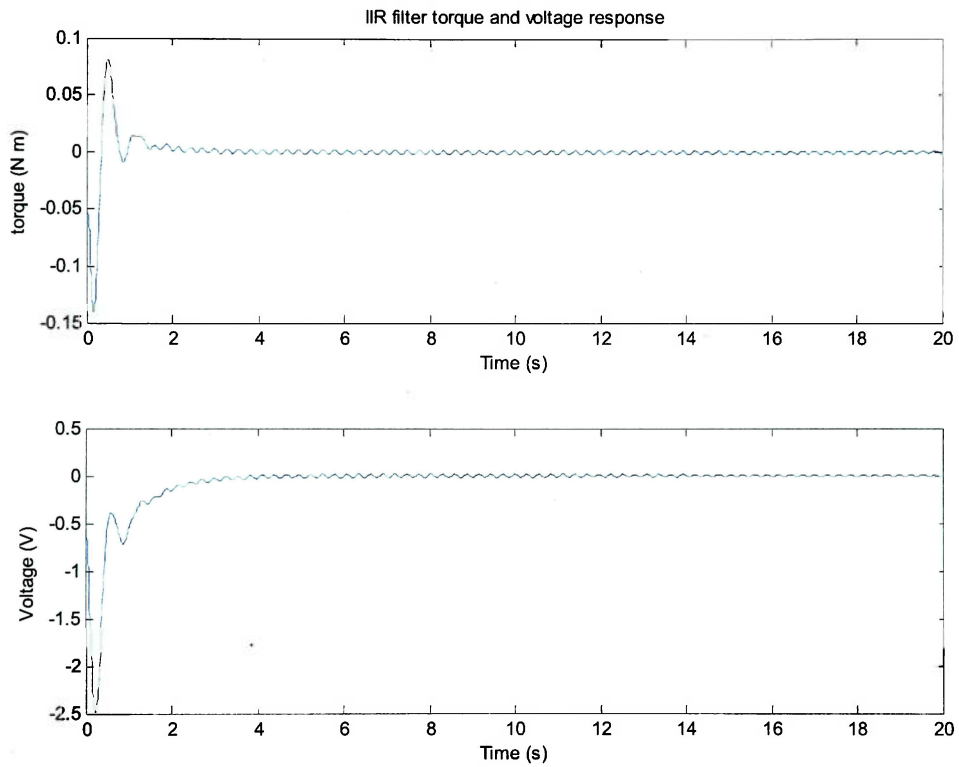


Figure 5.19. Case 2 PD Control with IIR filter τ and V_f responses.

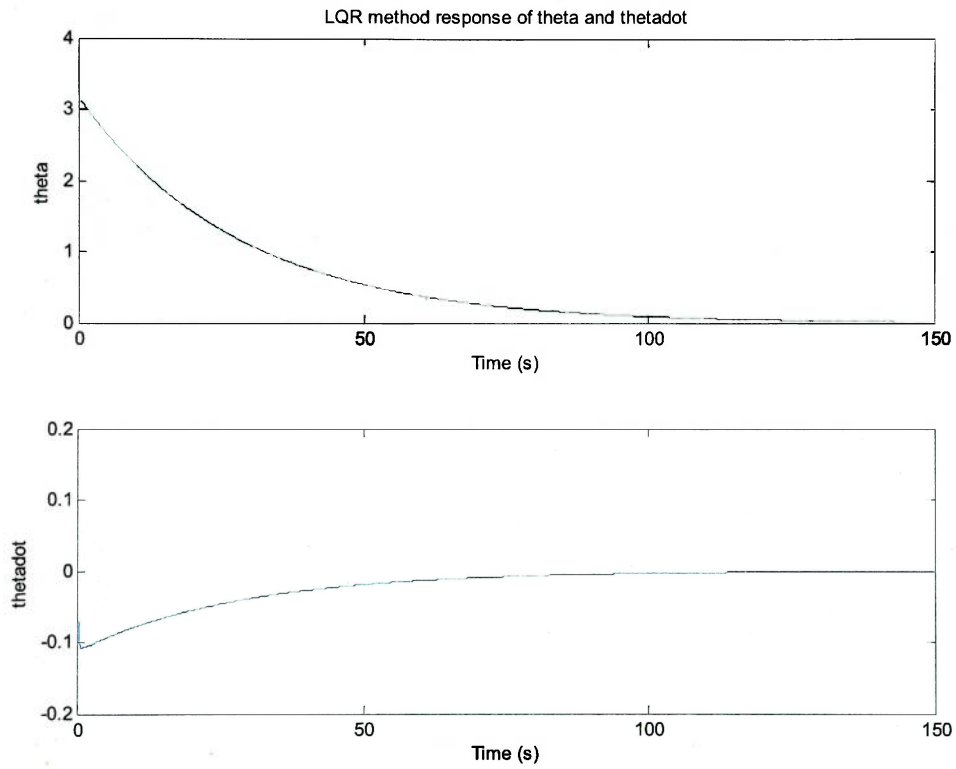


Figure 5.20. Case 2 LQR method θ and $\dot{\theta}$ responses.

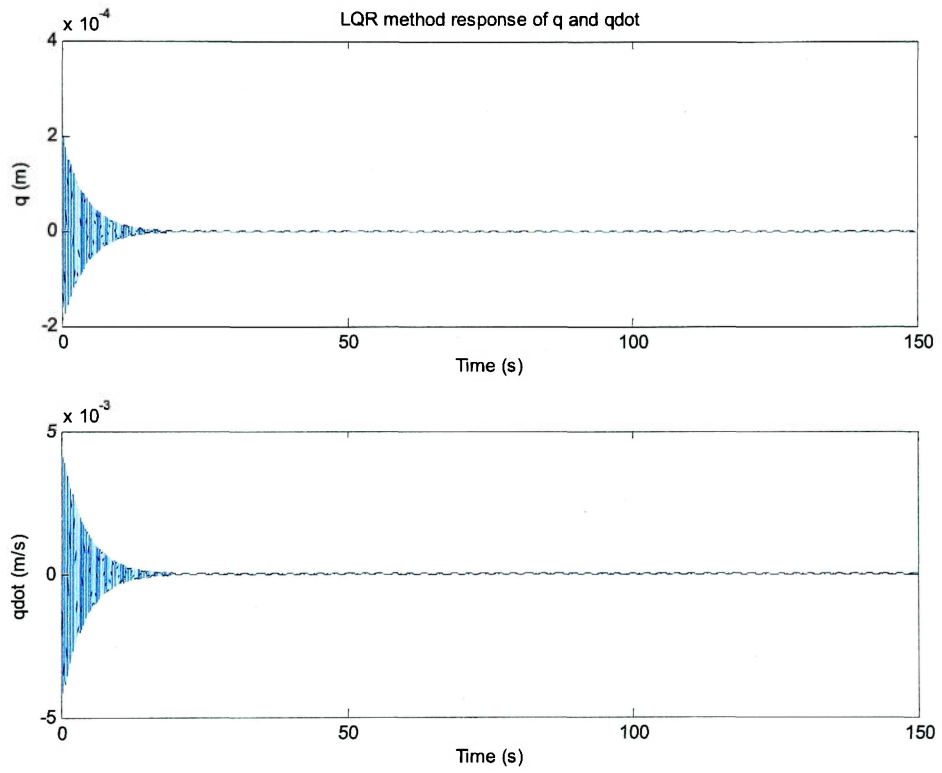


Figure 5.21. Case 2 LQR method q and \dot{q} responses.

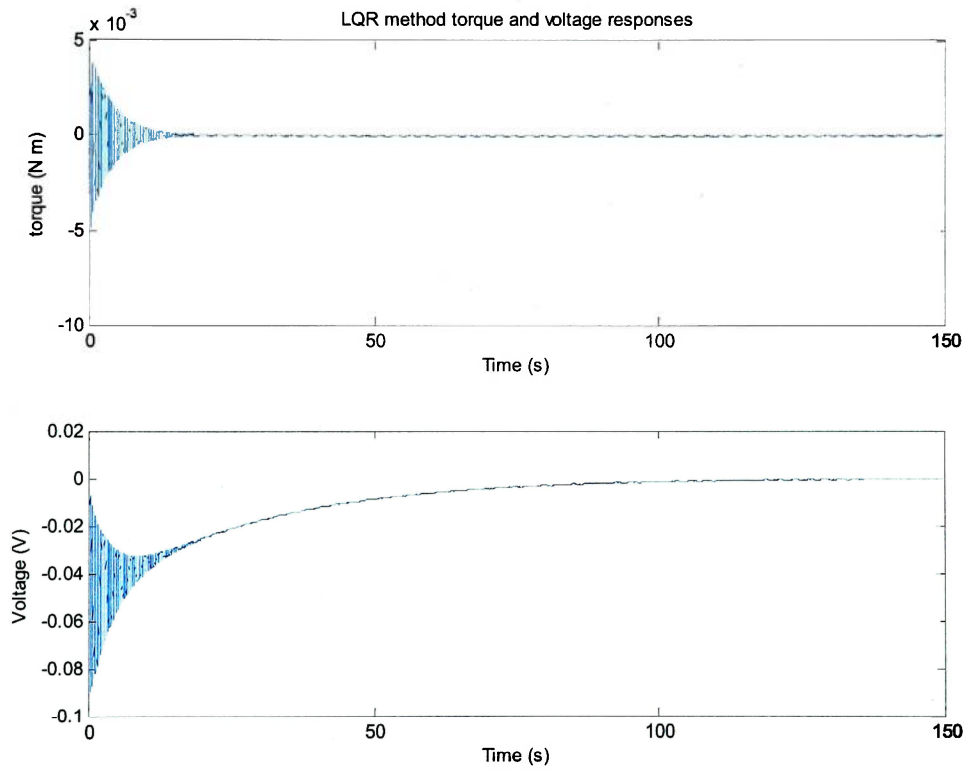


Figure 5.22. Case 2 LQR method τ and V_i responses.

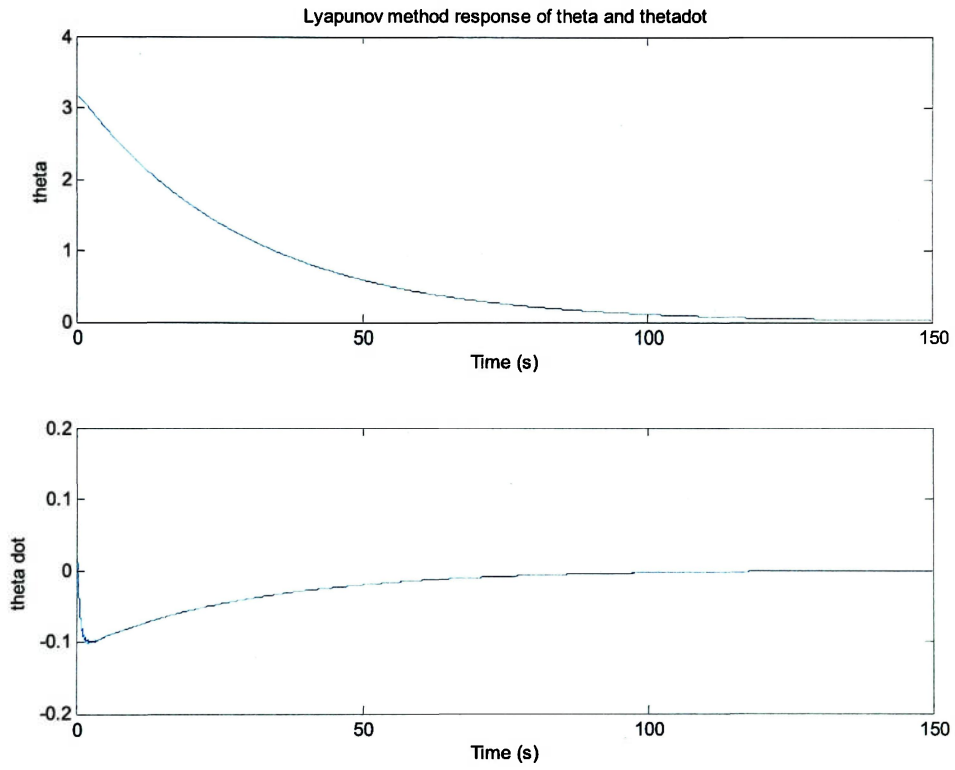


Figure 5.23. Case 2 Lyapunov method θ and $\dot{\theta}$ responses.

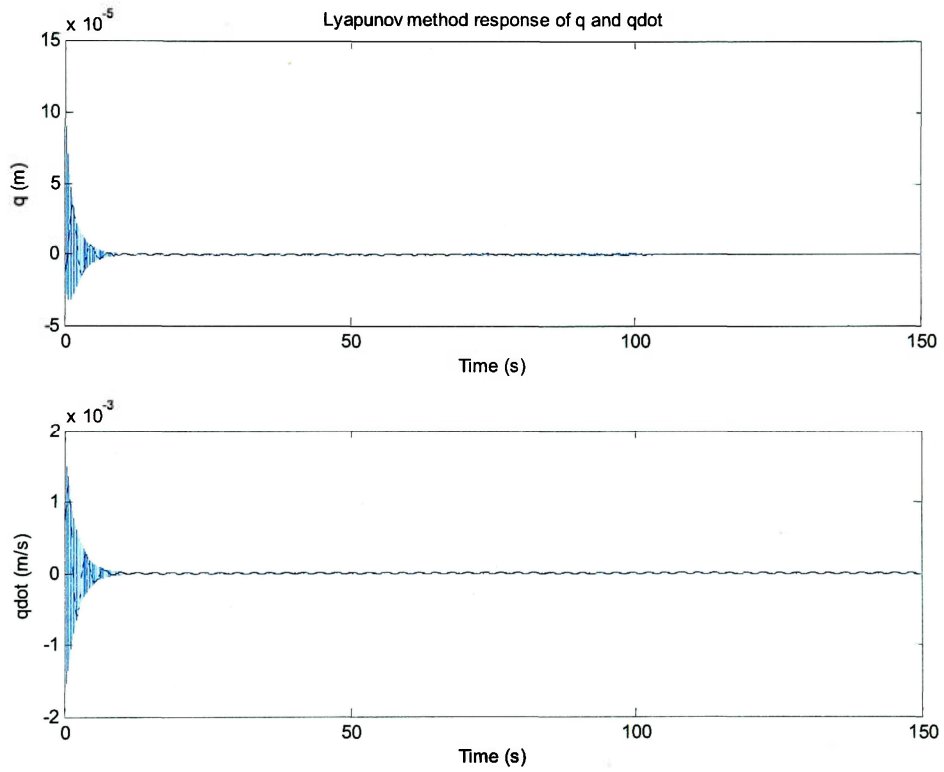


Figure 5.24. Case 2 Lyapunov method q and \dot{q} responses.

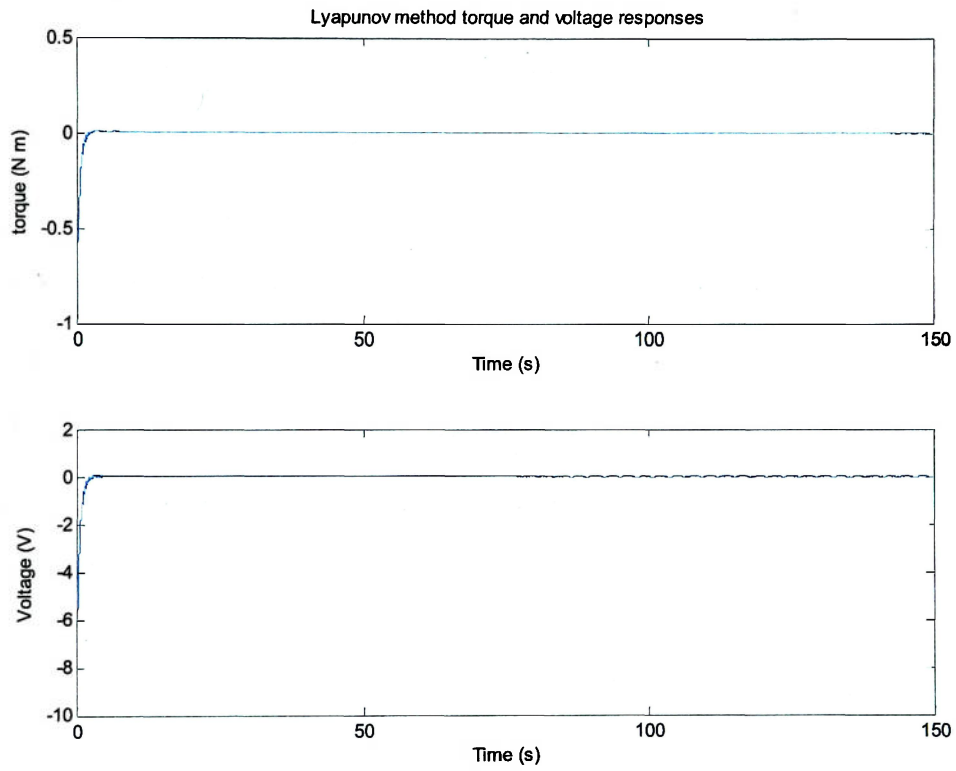


Figure 5.25. Case 2 Lyapunov method τ and V_i responses.

Chapter VI

Discussion of Results

6.1 Introduction

This chapter will review the performance of the controllers applied to the experimental setup. The figures do not all have the same time-axis scale, because of the filtered systems responded faster so their response would have been difficult to observe on the axes used for the LQR and Lyapunov-based designs.

6.2 Case 1: Filtered Control

As shown in Figures 5.2 and 5.5, the two filtered PD controlled systems, both the notch and IIR filters, performs rapid attitude changes for the systems in the first case in small amounts of time. The attitude θ for the rigid body quickly converges to the equilibrium state for both of the systems. Upon achieving the equilibrium, the systems remains at equilibrium for all subsequent times.

Figure 5.3 shows the deformation of the tip of the appendage for the notch filtered system peaked at magnitude of about 0.04 cm off the rigid body axis. The IIR filtered system's deformation, as shown in Figure 5.6, is about twice that of the notch filtered system. For both systems, after the time at which θ reached equilibrium, a subsequent small vibration is observed. This residual vibration is only on the order of a nanometer.

Figure 5.4 shows that the notch filtered system requires well within the allowable range of voltages for the motor to achieve the response as shown in Figure 5.2. Figure 5.7

shows the IIR filter system requires more voltage than the notch filter system, but still within the allowable range for the motor.

6.3 Case 1: LQR Control

As shown in Figure 5.8, the LQR method control responds much slower than the filtered controllers for the attitude change. The system behaves in a similar fashion like the filters after reaching the equilibrium attitude, as it remains there for all times afterwards.

The appendage tip motion, shown in Figure 5.9, performs better than the previous systems. The magnitude of the deflection is almost 10 times less than the filtered systems, with continued vibrating after reaching the desired attitude

Figure 5.10 shows that the voltage response for the LQR method is much less than that of the filtered systems, requiring on the order of 100 times less voltage for the motor for the maneuver.

6.4 Case 1: Lyapunov-Based Control

The Lyapunov-Based controller has a similar response time as the LQR method to achieve the equilibrium attitude. As seen in Figure 5.11, the systems remains at equilibrium for all subsequent times after reaching the equilibrium point.

The tip deflection for the Lyapunov method is near 100 times smaller in magnitude than the filtered system, and around 10 times less than the LQR system during the maneuver

to attitude equilibrium. Figure 5.12 also shows the frequency of the vibrations is much greater than the two filtered systems, but the amplitude of the vibrations is very small relative to the other systems.

Figure 5.13 shows that the voltage response for the Lyapunov-Based controller is well within the design parameters for the servo motor.

6.5 Case 2: Filtered Control

For Case 2, the filtered control designs responded similarly to case 1. Both of the systems' response times are in the range of case 1. As with Case 1, Figures 5.14 and 5.17 show that once the θ equilibrium point is achieved, the attitude of the system remains constant.

The filtered system designs break down for the large angle maneuver. Figures 5.15 and 5.18 show that both of the systems have residual vibrations after the equilibrium was reached. The amplitude of the vibration is about 1% of the maximum for the system, and remained for long durations after the equilibrium was achieved. This vibration is more apparent in the IIR tip deformation response.

As shown in Figures 5.16 and 5.19, the voltage response for both of the filters resides within the allowable ranges for the motor performance.

6.6 Case 2: LQR Control

Figure 5.20 shows that the LQR method has a response time similar to that of Case 1 for the attitude change in Case 2. As with Case 1, upon reaching the equilibrium attitude, the system remains stable.

The tip deflections shown in Figure 5.21 are again smaller in magnitude with respect to the filtered systems in Case 2. There is an apparent residual vibration of the system prior to reaching equilibrium, but it is much smaller than the residual vibrations after equilibrium is reached for the filtered systems.

Figure 5.22 shows that the required voltage response for the LQR method is again very low. This voltage is shown to be the smallest required voltage response for the Case 2 systems.

6.7 Case 2: Lyapunov-Based Control

Figure 5.23 shows that, as in Case 1, the Lyapunov-Based control for Case 2 has the slowest response time of all the systems. The Lyapunov-Based system is shown to remain stable after achieving the equilibrium point.

The tip deformation for the appendage is shown in Figure 5.24 to again be magnitudes smaller than the other proposed designs. There still exists a residual vibration in the system, but it can be seen that the deformation during the attitude change is minimal with respect to the rest of the system.

Figure 5.25 demonstrates that the Lyapunov-based design requires voltages within the range of the motor parameters.

Chapter VII

Conclusion

This thesis was focused on the design and application of a control method utilizing a Lyapunov-Based controller. Other controller designs were introduced to provide simple comparisons to the response of the Lyapunov control. The control designs were then applied using the physical parameters of an experimental setup and tested for validation of the designs.

The results of the application of the controllers to the experimental setup clearly show that under both small and large attitude control maneuvers, the Lyapunov-Based design outperformed the others presented in this thesis. The advantage of a Lyapunov-Based control over the other designs was also observed in the minimized deformation of the appendage during the maneuvers. The performance of this method would be expected to carry over to spaced-based applications as well.

Future research for this topic could include the purchase of the experimental setup described in this thesis. The setup is designed to work with the MATLAB software so the designs in this thesis could be directly applied to the system and validated through actual experimentation.

Bibliography

- [1] A. Banerjee, N. Pedreiro, and M. Gonzalez, "Simultaneous Optimization of Input Shaping and Feedback Control for Slewing Flexible Spacecraft," Proc. American Control Conf., 2003, pp.4796-4798.
- [2] A.E. Bryson Jr., Control of Spacecraft and Aircraft, Princeton University Press, New Jersey, 1994.
- [3] R.H. Cannon Jr. and D.E. Rosenthal, "Experiments in Control of Flexible Structures with Noncolocated Sensors and Actuators." AIAA Journal of Guidance, Control, and Dynamics, Vol.7, No.5, 1984, pp.546-553.
- [4] F. Casella, A. Locatelli, and N. Schiavoni, "Modeling and Control for Vibration Suppression in a Large Flexible Structure with Jet Thrusters and Piezoactuators," Proc. IEEE Conf. Decision and Control, 2000, pp.4491-4499.
- [5] C.A. Desoer and O. Morgul, "Control and Stabilization of a Flexible Beam Attached to a Rigid Body: Planar Motion," Proc. IEEE Conf. Decision and Control, 1988, pp.1643-1644.
- [6] S. Di Gennaro, "Output Attitude Control of Flexible Spacecraft from Quaternion Measures: a Passivity Approach," Proc. IEEE Conf. Decision and Control, 1998, pp.4549-4550.

- [7] S. Di Gennaro, "Output Stabilization of Flexible Spacecraft with Active Vibration Suppression," IEEE Transactions on Aerospace and Electronic Systems, Vol.39, No.3, 2003, pp.747-759.
- [8] S. Di Gennaro, "Attitude Tracking for Flexible Spacecraft from Quaternion Measures," Proc. IEEE Conf. Decision and Control, 2002, pp.4090-4091.
- [9] C.R. Dohrmann and R.D. Robinett, "Input Shaping for Three-Dimensional Slew Maneuvers of a Precision Pointing Flexible Spacecraft," Proc. IEEE Conf. Decision and Control, 1994, pp.2543-2547.
- [10] S.S. Ge, T.H. Lee, and L.F. Hong, "Robust Controller Design with Genetic Algorithm for Flexible Spacecraft," Proc. IEEE Conf. Decision and Control, 2001, pp.1033-1039.
- [11] S.S. Ge, T.H. Lee, and L.F. Hong, "Variable Structure Maneuvering Control of a Flexible Spacecraft," Proc. American Control Conf., 2001, pp.1599-1604.
- [12] S.S. Ge, T.H. Lee, and L.F. Hong, "Non-Model-Based Robust Controller Design for a Flexible Spacecraft," Proc. IEEE Conf. Decision and Control, 2000, pp.3785-3790.

[13] J.M. Hyde and W.P. Seering, "Using Input Command Pre-shaping to Suppress Multiple Mode Vibration," Proc. IEEE Conf. Robotics and Automation, 1991, pp.2604-2609.

[14] A. Iyer and S.N. Singh, "Variable Structure Attitude Control and Elastic Mode Stabilization of Flexible Spacecraft," Proc. IEEE Conf. Decision and Control, 1989, pp.809-814.

[15] S.M. Joshi and P.G. Maghami, "Robust Dissipative Compensators for Flexible Spacecraft Control." IEEE Transactions on Aerospace and Electronic Systems, Vol.28, No.3, 1992, pp.768-774.

[16] S.M. Joshi, P.G. Maghami, and A.G. Kelkar, "Design of Dynamic Dissipative Compensators for Flexible Space structures." IEEE Transactions on Aerospace and Electronic Systems, Vol.31, No.4, 1992, pp.1314-1324.

[17] J.L. Junkins and Y. Kim, Introduction to Dynamics and Control of Flexible Structures, AIAA Educational Series, 1993.

[18] A.G. Kelkar, S.M. Joshi, and T.E. Alberts, "Dynamic Dissipative Compensators for Multibody Flexible Space Structures." IEEE Transactions on Aerospace and Electronic

Systems, Vol.31, No.4, 1995, pp.1325-1330.

[19] A.G. Kelkar, S.M. Joshi, and T.E. Alberts, "Passivity-Based Control of Nonlinear Flexible Multibody Systems," IEEE Transactions on Automatic Control, Vol.40, No.5, 1995, pp.910-914.

[20] A.G. Kelkar and S.M. Joshi, "Global Stabilization of Multibody Spacecraft Using Quaternion-Based Nonlinear Control Law," Proc. American Control Conf., 1996, pp.3612-3615.

[21] H. Laosy, C.Z. Xu, and G. Sallet, "Boundary Feedback Stabilization of a Rotating Body-Beam System," IEEE Transactions on Automatic Control, Vol.41, No.2, 1996, pp.241-245.

[22] S.S. Lim and M. Farooq, "Slew-Maneuver Control for Large Flexible Spacecraft Under Random Noise," Proc. IEEE Conf. Decision and Control, 1992, pp.1297-1302.

[23] K.B. Lim, P.G. Maghami, and S.M. Joshi, "Comparison of Controller Designs for an Experimental Flexible Structure." IEEE Control Systems Magazine, 1992, pp.108-118.

[24] P. Lucibello, "Nonlinear Structurally Stable Control of a Flexible Spacecraft," Proc. IEEE Conf. Decision and Control, 1992, pp.1129-1134.

- [25] O. Morgul, "Dynamic boundary control of a Rotating Flexible Structure," Proc. IEEE Conf. Decision and Control, 1992, pp.1305-1310.
- [26] O. Morgul, "Orientation and Control of a Flexible Spacecraft: Planar Motion," Proc. IEEE Conf. Decision and Control, 1990, pp.393-394.
- [27] O. Morgul, "Orientation and Stabilization of a Flexible Beam Attached to a Rigid Body: Planar Motion," IEEE Transactions on Automatic Control, Vol.36, No.8, 1991, pp.953-962.
- [28] S.K. Nam and R.W. Zhang, "Fuzzy Multi-Variable Control for Attitude Stabilization of Flexible Spacecraft," Proc. IEEE Int. Conf. Intelligent Processing Systems, 1990, pp.257-261.
- [29] G.W. Neat, J.W. Melody, and B.J. Lurie, "Vibration Attenuation Approach for Spaceborne Optical Interferometers," IEEE Transactions on Control Systems Technology, Vol.6, No.6, 1998, pp.689-700.
- [30] M. Nohmi and M. Uchiyama, "Dynamics and 3-Axes Control of a Spacecraft with Flexible Structures," Proc. IEEE Conf. Decision and Control, 1996, pp.2695-2700.
- [31] K. Ogata, Modern Control Engineering, Prentice Hall, New Jersey 1997.

- [32] M. Reyhanoglu, "Model Truncation Effects in Variable Structure Control System Maneuvering of Flexible Spacecraft," M.S. Thesis, The Ohio State University, 1987.
- [33] T. Singh and W. Singhose, "Tutorial on Input Shaping/Time Delay Control of Maneuvering Flexible Structures," Proc. American Control Conf., 2002, pp.1717-1731.
- [34] U. Staehlin and T. Singh, "Design of Closed-Loop Input Shaping Controllers," Proc. American Control Conf., 2003, pp.5167-5172.
- [35] J. Watkins and S. Yurkovich, "Input Shaping Controllers for Slewing Flexible Structures," Proc. IEEE Conf. Decision and Control, 1992 pp.188-193.
- [36] B. Wie. Space Vehicle Dynamics and Control. AIAA Educational Series, 1998.